

## Volcanic Eruptions: Cyclicity during Lava Dome Growth

- 1 OLEG MELNIK<sup>1,2</sup>, R. STEPHEN J. SPARKS<sup>2</sup>,  
 2 ANTONIO COSTA<sup>2,3</sup>, ALEXEI A. BARMIN<sup>1</sup>  
 3 <sup>1</sup> Institute of Mechanics, Moscow State University,  
 4 Moscow, Russia  
 5 <sup>2</sup> Earth Science Department, University of Bristol,  
 6 Bristol, UK  
 7 <sup>3</sup> Istituto Nazionale di Geofisica e Vulcanologia,  
 8 Naples, Italy

### 9 Article Outline

- 10 Glossary  
 11 Definition of the Subject  
 12 Introduction  
 13 Dynamics of Magma Ascent During Extrusive Eruptions  
 14 Short-Term Cycles  
 15 Long-Term Cycles  
 16 Future Directions  
 17 Acknowledgments  
 18 Bibliography

### 19 Glossary

- 20 **Andesite** Magma or volcanic rock is characterized by in-  
 21 termediate SiO<sub>2</sub> concentration. Andesite magmas have  
 22 rheological properties that are intermediate between  
 23 basalt and rhyolite magmas. Silica content in andesites  
 24 ranges from approximately 52 to 66 weight percent.  
 25 Common minerals in andesite include plagioclase, am-  
 26 phibole and pyroxene. Andesite is typically erupted at  
 27 temperatures between 800 to 1000°C Andesite is par-  
 28 ticularly common in subduction zones, where tectonic  
 29 plates converge and water is introduced into the man-  
 30 tle.  
 31 **Basalt** Magma or volcanic rock contains not more than  
 32 about 52% SiO<sub>2</sub> by weight. Basaltic magmas have  
 33 a low viscosity. Volcanic gases can escape easily with-  
 34 out generating high eruption columns. Basalt is typi-  
 35 cally erupted at temperatures between 1100 to 1250°C.  
 36 Basalt flows cover about 70% of the Earth's surface and  
 37 huge areas of the terrestrial planets and so are the most  
 38 important of all crustal igneous rocks.  
 39 **Bingham liquid** is a fluid that does not flow in response  
 40 to an applied stress until a critical yield stress is  
 41 reached. Above the critical yield stress, strain rate is  
 42 proportional to the applied stress, as in a Newtonian  
 43 fluid.

**Bubbly flow** A multi-phase flow regime, in which the gas  
 phase appears as bubbles suspended in a continuous  
 liquid phase.

**Conduit** A channel, through which magma flows towards  
 the Earth's surface. Volcanic conduits can commonly  
 be approximately cylindrical and typically a few 10's  
 meters across or bounded by near parallel sides in  
 a magma-filled fracture. Conduits can be vertical or in-  
 clined.

**Crystallization** Conversion, partial or total, of a silicate  
 melt into crystals during solidification of magma.

**Degassing n. (degas v.)** The process by which volatiles  
 that are dissolved in silicate melts come out of solu-  
 tion in the form of bubbles. Open- and closed-system  
 degassing can be distinguished. In the former, volatiles  
 can be lost or gained by the system. In the latter, the  
 total amount of volatiles in the bubbles and in solution  
 in the magma is conserved.

**Differentiation** The process of changing the chemical  
 composition of magma by processes of crystallization  
 accompanied by separation melts from crystals.

**Dome** A steep-sided, commonly bulbous extrusion of  
 lava or shallow intrusion (cryptodome). Domes are  
 commonly, but not exclusively, composed of SiO<sub>2</sub>-  
 rich magmas. In dome-forming eruptions the erupted  
 magma is so viscous, or the discharge rate so slow,  
 that lava accumulates very close to the vent region,  
 rather than flowing away. Pyroclastic flows can be gen-  
 erated by collapse of lava domes. Recent eruptions pro-  
 ducing lava domes include the 1995–2006 eruption of  
 the Soufrière Hills volcano, Montserrat, and the 2004–  
 2006 eruption of Mount St. Helens, USA.

**Dyke** A sheet-like igneous intrusion, commonly vertical  
 or near vertical, that cuts across pre-existing, older, ge-  
 ological structures. During magmatism, dykes trans-  
 port magma toward the surface or laterally in fracture-  
 like conduits. In the geologic record, dykes are pre-  
 served as sheet-like bodies of igneous rocks.

**Explosive eruption** A volcanic eruption in which gas ex-  
 pansion tears the magma into numerous fragments  
 with a wide range of sizes. The mixture of gas and  
 entrained fragments flows upward and outward from  
 volcanic vents at high speed into the atmosphere. De-  
 pending on the volume of erupted material, erup-  
 tion intensity and sustainability, explosive eruptions  
 are classified as Strombolian, Vulcanian, sub-Plinian,  
 Plinian or Mega-Plinian; this order is approximately  
 in the order of increasing intensity. Strombolian and  
 Vulcanian eruptions involve very short-lived explo-  
 sions.

Please note that the pagination is not final; in the print version an entry will in general not start on a new page.

- 94 **Extrusive flow or eruption** A non-explosive (non-pyro- 145  
95 clastic) magma flow from a volcanic conduit during 146  
96 a lava dome-building eruption or lava flow. 147
- 97 **Mafic** Magma, lava, or tephra with silica concentrations 148  
98 of approximately  $\text{SiO}_2 < 55\%$ . 149
- 99 **Magma** Molten rock that consists of up three compo- 150  
100 nents: liquid silicate melt, suspended crystalline solids, 151  
101 and gas bubbles. It is the raw material of all vol- 152  
102 canic processes. Silicate magmas are the most common 153  
103 magma type and consist of long, polymeric chains and 154  
104 rings of Si–O tetrahedra, between which are located 155  
105 cations (e. g.  $\text{Ca}^{2+}$ ,  $\text{Mg}^{2+}$ ,  $\text{Fe}^{2+}$ , and  $\text{Na}^+$ ). Anions (e. g. 156  
106  $\text{OH}^-$ ,  $\text{F}^-$ ,  $\text{Cl}^-$ , and  $\text{S}^-$ ) can substitute for the oxygen 157  
107 in the silicate framework. The greater the silica ( $\text{SiO}_2$ ) 158  
108 content of the magma, the more chains and rings of 159  
109 silicate tetrahedra there are to impede each other and 160  
110 hence the viscosity of the magma increases. The pres- 161  
111 sure regime and composition of the magma control the 162  
112 minerals that nucleate and crystallize from a magma 163  
113 when it cools or degasses. 164
- 114 **Magma chamber** A subsurface volume within which 165  
115 magma accumulates, differentiates and crystallizes. Ig- 166  
116 neous intrusions can constrain the form and size of 167  
117 some magma chambers, but in general the shape and 168  
118 volume of magma chambers beneath active volcanoes 169  
119 are poorly known. Magma reservoir is an equivalent 170  
120 term. 171
- 121 **Melt** Liquid part of magma. Melts (usually silicate) con- 172  
122 tain variable amounts of dissolved volatiles. The pri- 173  
123 mary volatiles are usually water and carbon dioxide. 174
- 124 **Newtonian liquid** A liquid for which the strain rate is 175  
125 proportional to the applied stress. The proportionality 176  
126 coefficient is called the viscosity. 177
- 127 **Microlite** Crystal with dimensions less than  $100\ \mu\text{m}$ . Usu- 178  
128 ally microlites crystallize at shallow levels of magmatic 179  
129 system. 180
- 130 **Phenocryst** Crystal with dimensions larger than  $100\ \mu\text{m}$ . 181  
131 Usually phenocrysts grow in magmatic reservoirs prior 182  
132 to an eruption and or are entrained by magma in the 183  
133 chamber. 184
- 134 **Pyroclastic flow or surge** A gas-particle flow of pyro- 185  
135 clasts suspended in a mixture of hot air, magmatic 186  
136 gas, and fine ash. The flow originates by the gravita- 187  
137 tional collapse of a dense, turbulent explosive eruption 188  
138 column at the source vent, or by dome collapse, and 189  
139 moves down-slope as a coherent flow. Pyroclastic flows 190  
140 and surges are distinguished by particle concentration 191  
141 in the flow, surges being more dilute. Variations in par-  
142 ticle concentration result in differences in the deposits  
143 left by flows and surges.
- 144 **Silicic** Magma, lava, or tephra with silica concentrations  
of approximately  $\text{SiO}_2 > 55\%$ . The magmas are com-  
monly rich in Al, Na– and K– bearing minerals. Sili-  
cic magmas are typically very viscous and can have  
high volatile contents. Rhyolite is an example of a sili-  
cic magma.
- Volatile** A component in a magmatic melt which can be  
partitioned in the gas phase in significant amounts  
during some stage of magma history. The most com-  
mon volatile in magmas is water vapor  $\text{H}_2\text{O}$ , but there  
are commonly also significant quantities of  $\text{CO}_2$ ,  $\text{SO}_2$   
and halogens.

### Definition of the Subject

We consider the process of slow extrusion of very viscous magma that forms lava domes. Dome-building eruptions are commonly associated with hazardous phenomena, including pyroclastic flows generated by dome collapses, explosive eruptions and volcanic blasts. These eruptions commonly display fairly regular alternations between periods of high and low or no activity with time scales from hours to years. Usually hazardous phenomena are associated with periods of high magma discharge rate, thus, understanding the causes of pulsatory activity during extrusive eruptions is an important step towards forecasting volcanic behavior, especially the transition to explosive activity when magma discharge rate increases by a few orders of magnitude. In recent years the risks have increased because the population density in the vicinity of many active volcanoes has increased.

### Introduction

Many volcanic eruptions involve the formation of lava domes, which are extrusions of very viscous, degassed magmas. The magma is so viscous that it accumulates close to the vent. Extrusion of lava domes is a slow and long-lived process, and can continue for many years or even decades [71,83,85]. Typical horizontal dimensions of lava domes are several hundred meters, heights are of an order of tens to several hundred meters, and volumes several million to hundreds of million cubic meters. Typical magma discharge rates (measured as the increase of dome volume with time in dense rock equivalent (DRE)) can reach up to  $20\text{--}40\ \text{m}^3/\text{s}$ , but are usually below  $10\ \text{m}^3/\text{s}$  [83].

Dome-building eruptions are commonly associated with hazardous phenomena, including pyroclastic flows and tsunamis generated by dome collapses, explosive eruptions and volcanic blasts. Dome-building eruptions can also contribute to edifice instability and sector collapse, as occurred on Montserrat on 26 December

1997 [87]. Lava dome activity can sometimes precede or follow major explosive eruptions; the eruption of Pinatubo, Philippines (1991) is an example of the former [37], and the eruption of Mount St. Helens, USA (1980–1986) is an example of the latter [89].

Several lava dome eruptions have been documented in detail and show quite complex behaviors. Substantial fluctuations in magma discharge rate have been documented. In some cases these fluctuations can be quite regular (nearly periodic), as in the extrusion of lava in 1980–1982 on Mount St. Helens [89] and in the 1922–2002 activity of the Santiaguito lava dome, Guatemala [35]. In these cases, periods of high magma discharge rate alternate with longer periods of low magma discharge rate or no extrusion. In some volcanoes, such as Shiveluch, Kamchatka, the intervals of no extrusion are so long compared with the periods of dome growth that the episodes of dome growth have been described as separate eruptions of the volcano rather than episodes of the same eruption. Other dome-building activity can be nearly continuous and relatively steady, as observed at Mount St. Helens in 1983 [89] and at the Soufrière Hills Volcano, Montserrat between November 1999 and July 2003. In yet other cases the behavior can be more complex with quite sudden changes in magma discharge rate, which cannot be related to any well-defined regularity or pattern (e. g. Lascar volcano, Chile, [57]).

Pauses during lava dome-building eruptions are quite common. For example, at Mount St. Helens there were 9 pulses of dome growth with a period of  $\sim 74$  days, a duration of 1–7 days and no growth in between [89]. The Soufrière Hills Volcano Montserrat experienced a long (20 months) pause in extrusion after the first episode of growth [72]. On Shiveluch volcano in Kamchatka episodes of dome growth occurred in 1980, 1993 and 2000, following a major explosion in 1964 [28]. Each episode of dome growth began with magma discharge rate increasing over the first few weeks to a peak of 8–15 m<sup>3</sup>/s, with a gradual decline in magma discharge rate over the following year. In between the episodes very minimal activity was recorded.

Fluctuations in magma discharge rate have been documented on a variety of time-scales from both qualitative and quantitative observations. Several lava dome eruptions are characterized by extrusion of multiple lobes and flow units [68,94]. In the case of the Soufrière Hills Volcano, extrusion of shear lobes can be related to spurts in discharge rate and is associated with other geophysical changes, such as onset of seismic swarms and marked changes in temporal patterns of ground tilt [90,91,94]. These spurts in discharge rate have been fairly regular for substantial periods, occurring every 6 to 7 weeks over

a 7 month period in 1997 [21,87,91]. These spurts are commonly associated with large dome collapses and pyroclastic flows and, in some cases, with the onset of periods of repetitive Vulcanian explosions [14,26]. Consequently the recognition of this pattern has become significant for forecasting activity for hazard assessment purposes. In the Soufrière Hills Volcano and Mount Pinatubo much shorter fluctuations in magma discharge rate have been recognized from cyclic variations in seismicity, ground tilt, gas fluxes and rock-fall activity [23,91,93]. This cyclic activity has typical periods in the range of 4 to 36 hours. Cyclic activity has been attributed to cycles of gas pressurization and depressurization with surges in dome growth related to degassing, rheological stiffening and stick-slip behavior [23,49,61,91,98].

Dome eruptions can show transitions to explosive activity, which sometimes can be linked to spurts in magma discharge rate. For example, in 1980, periodic episodes of lava dome extrusion on Mount St. Helens were initiated by explosive eruptions, which partly destroyed the dome that had been extruded in each previous extrusion episode [89]. At Unzen Volcano, Japan a single Vulcanian explosive eruption occurred in June 1991 when the magma discharge rate was at its highest [68]. At the Soufrière Hills Volcano, repetitive series of Vulcanian explosions have occurred following large dome collapses in periods when magma discharge rates were the highest of the eruption [26,88]. In the case of Lascar Volcano, Chile, an intense Plinian explosive eruption occurred on 18 and 19 April, 1993, after nine years of dome extrusion and occasional short-lived Vulcanian explosions [57].

Lava dome eruptions require magma with special physical properties. In order to produce a lava dome rather than a lava flow, the viscosity of the magma must be extremely high so that the lava cannot flow easily from the vent. High viscosity is a consequence of factors such as relatively low temperature (typically 750–900°C), melt compositions rich in network-forming components (principally Si and Al) efficient gas loss during magma decompression, and crystallization as a response to cooling and degassing. Viscosities of silica-rich magmas, such as rhyolites and some andesites, are increased by several orders of magnitude by the loss of dissolved water during decompression. Many, but not all, domes also have high crystal content (up to 60 to 95 vol%), with crystallization being triggered mostly by degassing [10,86]. In order to avoid fragmentation that leads to an explosive eruption, magma must have lost gas during ascent. Consider, for example, a magma at 150 MPa containing 5wt% of dissolved water decompressed to atmospheric pressure. Without gas loss the volume fraction of bubbles, will be more than

99%. Typical dome rock contains less than 20 vol% of bubbles, although there is evidence that magma at depth can be more bubble-rich (e. g., [13,74]). On the other hand, very commonly there is no change in temperature or bulk magma composition in the products of explosive and extrusive eruptions for a particular volcano. This suggests that the properties of magma that are conducive to the formation of lava domes are controlled by physico-chemical transformations that occurred during magma ascent to the surface.

Two other important factors that influence whether lava domes or flows form are topography and discharge rate. The same magma can form a dome if the discharge rate is low, and a lava flow if the rate is high [29,92]. The discharge rate is controlled by overall conduit resistance that is a function of viscosity, conduit size and shape, and driving pressure (the difference between chamber pressure and atmospheric pressure). Additionally the same magma can form a dome on low slopes, such as a flat crater (e. g. the mafic andesite dome of the Soufrière Volcano, St. Vincent; [40]) and a lava flow on steep slopes.

Prior to an eruption, magma is usually stored in a shallow crustal reservoir called a magma chamber. For several volcanoes magma chambers can be detected and characterized by earthquake locations, seismic tomography, petrology or interpretation of ground deformation data [55]. Typical depths of magma chambers range from a few kilometers to tens of kilometers. Volumes range from less than one to several thousand km<sup>3</sup> [55], but are usually less than a hundred km<sup>3</sup>. Magma chambers are connected to the surface by magma pathways called conduits. There is evidence that the conduits that feed lava dome eruptions can be both dykes or cylindrical. Dykes of a few meters width are commonly observed in the interior of eroded andesite volcanoes. Dyke feeders to lava domes have been intersected by drilling at Inyo crater, California, USA [56] and at Mount Unzen [67]. Geophysical studies point to dyke feeders; for example fault-plane solutions of shallow volcano-tectonic earthquakes indicate pressure fluctuations in dykes [75,76]. Deformation data at Unzen, combined with structural analysis, indicate that the 1991–1995 dome was fed by a dyke [68]. Dykes are also the only viable mechanism of developing a pathway through brittle crust from a deep magma chamber to the surface in the initial stages of an eruption [50,77].

Cylindrical conduits commonly develop during lava dome eruptions. The early stages of lava dome eruptions frequently involve phreatic and phreatomagmatic explosions that create near surface craters and cylindrical conduits [12,73,87,89,96,99]. These explosions are usually attributed to interaction of magma rising along a dyke with

ground water. Cylindrical conduits formed by explosions are confined to relatively shallow parts of the crust, probably of order hundreds of meters depth and < 1 km, as indicated by mineralogical studies [73]. Examples of such initial conduit forming activity include Mount Usu (Japan) Mt. St. Helens, and Soufrière Hills Volcano [12,87,99]. Many lava dome eruptions are also characterized by Vulcanian, sub-Plinian and even Plinian explosive eruptions. Examples include Mount Unzen, Mount St. Helens, Santiaguito and Soufrière Hills Volcano [68,87,89,96]. Here the fragmentation front may reach to depths of several kilometers [54] with the possibility of cylindrical conduit development due to severe underpressurization and mechanical disruption of conduit wallrocks. Subsequently domes can be preferentially fed along the cylindrical conduits created by earlier explosive activity. On the Soufrière Hills Volcano, early dome growth was characterized by extrusion of spines with nearly cylindrical shape [87].

Observations of magma discharge rate variations on a variety of time-scales highlight the need to understand the underlying dynamic controls. Research has increasingly focused on modeling studies of conduit flow dynamics during lava-dome eruptions. We will restrict our discussions here to mechanisms that lead to cyclic and quasi-periodic fluctuations in magma discharge rate on various timescales, mainly focusing on long-term cycles. Issues concerning the transition between explosive and extrusive activity are discussed in detail in [45,80,81,97] and in the special volume of *Journal of Volcanology and Geothermal Research* dedicated to modeling of explosive eruptions [79]. Several papers consider the processes that occur at the surface and relate dome morphology and dimensions with controlling parameters.

Combined theoretical, experimental and geological studies identify four main types of dome: spiny, lobate, platy, and axisymmetric [5,29,30]. These types of dome reflect different regimes which are controlled by discharge rates, cooling rates and yield strength, and the viscosity of the dome-forming material. In recent years mathematical modeling has been used to semi-quantitatively describe spreading of lava domes, including models based on the thin layer approximation [1,2] and fully 2D simulations of lava dome growth which account for visco-elastic and -plastic rheologies [32,33].

### Dynamics of Magma Ascent During Extrusive Eruptions

In order to understand the causes of cyclic behavior during extrusive eruptions, first we need to consider the un-



derling dynamics of volcanic systems, and discuss physical and chemical transitions during magma ascent.

The physical framework for the model of a volcanic system is shown in Fig. 1. Magma is stored in a chamber at depth  $L$ , with a chamber pressure  $P_{\text{ch}}$  that is higher than hydrostatic pressure of magma column and drives magma ascent. Magma contains silicate melt, crystals and dissolved and possibly exsolved volatiles. During ascent of the magma up the conduit the pressure decreases and volatiles exsolve forming bubbles. As the bubble concentration becomes substantial, bubble coalescence take place and permeability develops [27,45], allowing gas to escape from ascending magma, both in vertical (through the magma) and horizontal (to conduit wallrocks) directions. If magma ascends slowly, gas escape results in a significant reduction of the volume fraction of bubbles; such a process is termed open system degassing. In comparison closed system degassing is characterized by a negligible gas escape. Reduction in bubble content, combined with relatively low gas pressures and efficient decoupling of the gas and melt phases, prevents magma fragmentation and, thus, development of explosive eruption [59,60,82].

Due to typical low ascent velocities (from millimeters to a few centimeters per second) magma ascent times to the Earth's surface from the magma chamber range from a several hours to many weeks. These ascent times are often comparable with the times that are required for crystals to grow significantly and for heat exchange between magma and wallrocks. The main driving force for crystallization is related to exsolution of volatiles from the magma, leading to increase in the liquidus temperature  $T_L$ , and development of magma undercooling  $\Delta T = T_L - T$  [10]. Crystallization leads to release of latent heat, and magma temperature can increase with respect to the initial temperature [6]. As a consequence of increasing crystal content, magma viscosity increases by several orders of magnitude [16,20,21] and magma becomes a non-Newtonian fluid [78]. As will be shown later, crystallization induced by degassing can become a key process in causing variable flow rates.

Due to the long duration of extrusive eruptions, the magma chamber can be replenished with significant amounts of magma from underlying sources [41,65]. Replenishment can lead to pressure build-up in the magma chamber, volatile and heat exchange between host and new magmas. The composition of the magma can also change over time, due to differentiation, crustal rock assimilation, or magma mixing. Thus, any model that explains magma ascent dynamics needs to deal with many complexities. Of course there is no single model that can take into account all physical processes in a volcanic system. Addi-

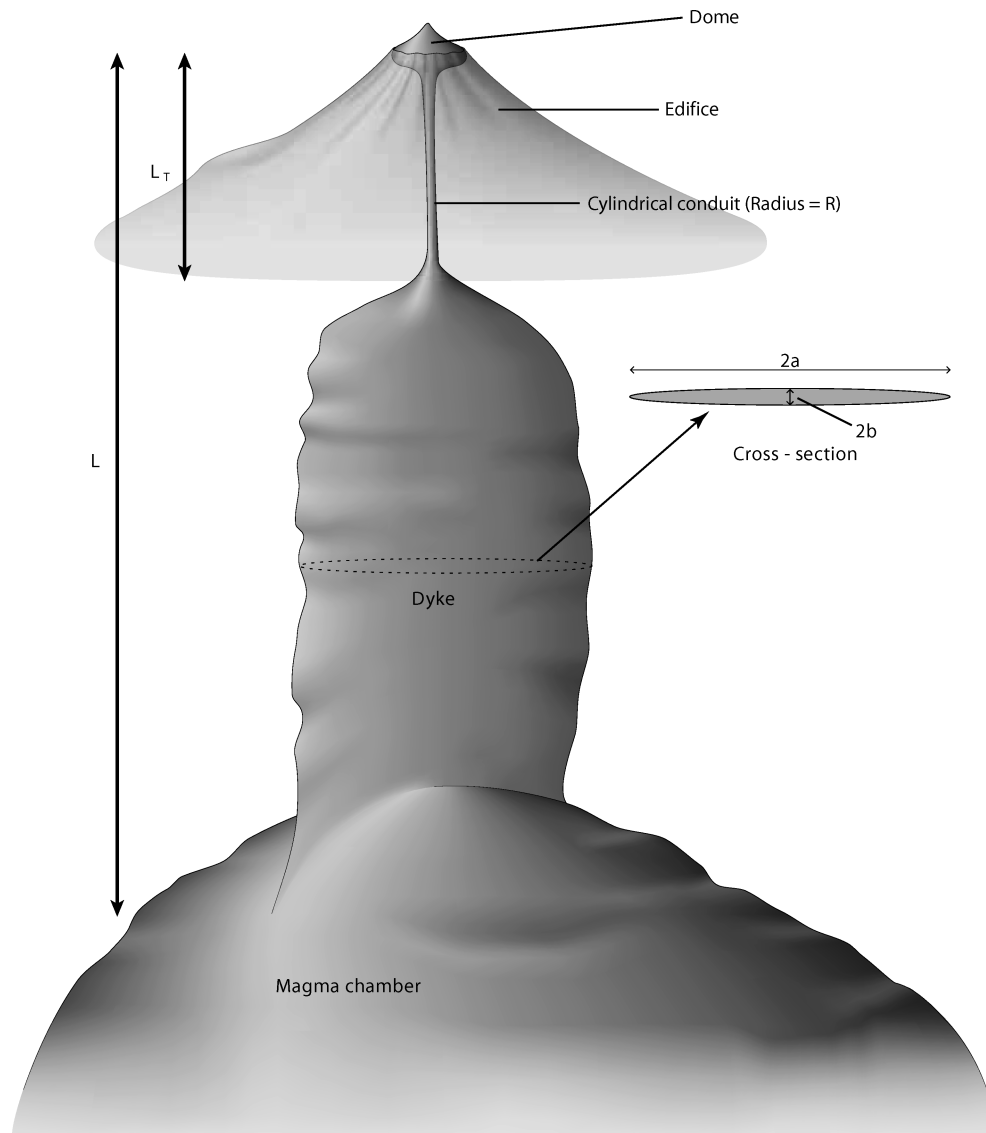
tional complications arise from the fact that the physical properties of magma at high crystal contents, such as rheology or crystal growth kinetics and geometry of volcanic systems, are typically poorly constrained. Several issues regarding the dynamics of multiphase systems have not been resolved theoretically, especially for cases where the volume fractions of components of the multiphase system are comparable.

Below we will present a review of existing models that treat cyclic behavior during extrusive eruptions on different timescales.

### Short-Term Cycles

Cyclic patterns of seismicity, ground deformation and volcanic activity (Fig. 2 from [23]) have been documented at Mount Pinatubo, Philippines, in 1991 [37] and Soufrière Hills volcano, Montserrat, British West Indies, in 1996–1997 [90,91]. At Soufrière Hills, periodicity in seismicity and tilt ranged from  $\sim 4$  to 30 h, and the oscillations in both records continued for weeks. Cyclic behavior was first observed in the seismicity (RSAM) records beginning in July 1996, when the record of dome growth constrained the average supply rate to between 2 and 3  $\text{m}^3/\text{s}$  [88]. The oscillations in the RSAM records initially had low amplitudes, and no tilt-measurement station was close enough to the vent to detect any pressure oscillations in the conduit. By August 1996, RSAM records showed strong oscillatory seismicity at dome-growth rates between 3 and 4  $\text{m}^3/\text{s}$ . Tilt data, taken close enough to the vent (i. e., Chances Peak [90]) to be sensitive to conduit pressure oscillations, are only available for February 1997 and May–August 1997. In the latter period dome growth rate increase from  $\sim 5$   $\text{m}^3/\text{s}$  in May to between 6 and 10  $\text{m}^3/\text{s}$  in August. Both near-vent tilt and RSAM displayed oscillatory behavior during this period and were strongly correlated in time. Similar RSAM oscillations having periods of 7 to 10 h were observed at Mount Pinatubo following the climactic eruption in 1991 [37]. At both volcanoes, oscillation periods were observed that do not fit any multiple of Earth or ocean tides.

The cyclic activity at both Pinatubo and Soufrière Hills Volcano are strongly correlated with eruptive behavior and other geophysical phenomena. In the Pinatubo case and on Soufrière Hills Volcano in August, September and October 1997, the cycles were linked to short-lived volcanic explosions. In the case of the Soufrière Hills Volcano, explosions in August 1997 occurred at the peak in the tilt. The peak in tilt also marked the onset of episodes of increased rock falls [7,8] and [91] is attributed to increased magma discharge rates.  $\text{SO}_2$  flux data show that the cy-



**Volcanic Eruptions: Cyclicity during Lava Dome Growth, Figure 1**

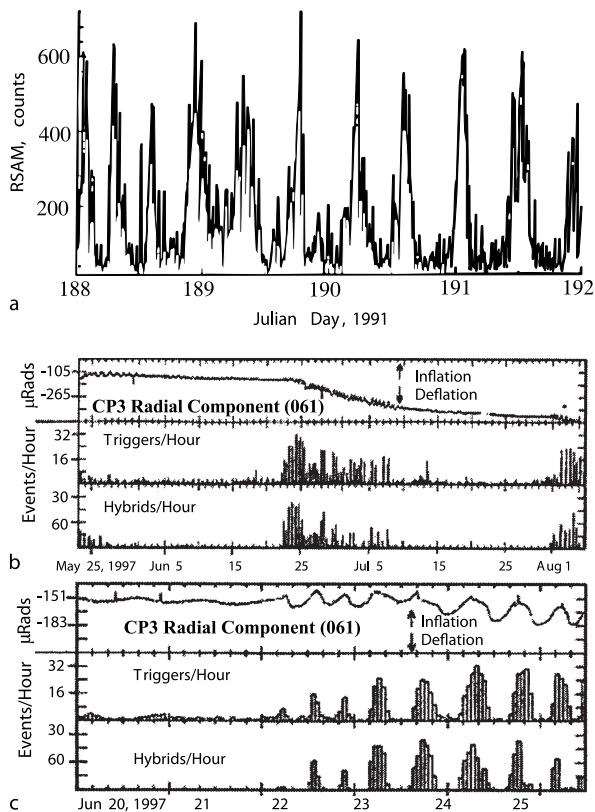
Schematic view of the volcanic system. In the upper part the conduit is cylindrical with a radius  $R$ . A transition from the cylinder to a dyke occurs at depth  $L_T$ . The length scale for the transition from cylinder to dyke is  $w_T$ . The dyke has an elliptical cross-section with semi-axis lengths  $a_0$  and  $b_0$ . The chamber is located a depth  $L$ . In the text we used also the following auxiliary variables:  $D = 2R$  for conduit diameter,  $L_d = L - L_T$  for the dyke vertical length,  $W_d = 2a_0$  for the dyke width, and  $H_d = 2b_0$  for the dyke thickness. After [20]

cles are linked to surges in gas release, which reach a peak about an hour after the tilt peak [93]. Green et al. [31] have shown that several families of near identical long period earthquakes occur during the tilt cycle, starting at the inflexion point on the up-cycle and finishing before the inflexion point on the down-cycle.

Several models [23,49,70,98,98] have been proposed to explain the observed cyclicity. In these models [23,98] the

conduit is divided into two parts. Magma is assumed to be forced into the lower part of volcanic conduit at a constant rate. In Denlinger and Hoblitt [23] magma in the lower part of the conduit is assumed to be compressible. In Wylie et al. [98] the magma is incompressible but the cylindrical conduit is allowed to expand elastically. In both models the lower part of the conduit, therefore, acts like a capacitor that allows magma to be stored temporarily in

501  
502  
503  
504  
505  
506  
507  
508



**Volcanic Eruptions: Cyclicity during Lava Dome Growth, Figure 2**  
 Examples of cyclic behavior in a lava dome eruption. RSAM records from Mt. Pinatubo, Philippines following its climatic eruption in June 1991 (a, after [23]). Radial tilt, triggered earthquakes, and hybrid earthquakes for 17 May to 6 August 1997, at Soufrière Hills Volcano (b, after [21,90]). Parts of three 5–7 week cycles are shown, with each cycle showing high amplitude tilt and seismicity pulsations with short time scale that last for several weeks after the start of the cycle. The onset of a cycle is rapid, as detailed in c for the cycle initiating on 22 June 1997

order to release it during the intense phase of the eruption. In the upper part of the conduit friction is dependent on magma discharge rate, with a decrease in friction resulting in an increase in discharge rate, over a certain range of discharge rates. In Denlinger and Hoblitt [23], when magma discharge rate reaches a critical value, magma detaches from the conduit walls and a stick-slip transition occurs. Rapid motion of magma leads to depressurization of the conduit and a consequent decrease in discharge rate, until at another critical value the magma again sticks to the walls. Pressure starts to increase again due to influx of new magma into the conduit. On a pressure-discharge diagram the path of eruption is represented by a hysteresis loop. In Wylie et al. [98] the friction is controlled by volatile-dependent viscosity. Volatile exsolution delay is controlled

by diffusion. When magma ascends rapidly, volatiles have no time to exsolve and viscosity remains low. Depressurization of the upper part of the conduit leads to a decrease in magma discharge rate and an increase in viscosity due to more intense volatile exsolution.

In Neuberg et al. [70] a steady 2D conduit flow model was developed. The full set of Navier–Stokes equations for a compressible fluid with variable viscosity was solved by means of a finite element code. Below some critical depth the flow was considered to be viscous and Newtonian, with a no-slip boundary condition at the wall. Above this depth a plug develops, with a wall boundary condition of frictional slip. The slip criterion was based on the assumption that the shear stress inside the magma overcomes some critical value. Simulations reveal that slip occurs in the shallow part of the conduit, in good agreement with locations of long-period volcanic earthquakes for the Soufrière Hills Volcano, [31]. However, some parameters used in the simulations (low crystallinity, less than 30% and high discharge rate, more than  $100 \text{ m}^3/\text{s}$ ) are inconsistent with observations.

Lensky et al. [49] developed the stick-slip model by incorporating degassing from supersaturated magma together with a sticking plug. Gas diffuses into the magma, which cannot expand due to the presence of a sticking plug, resulting in a build up of pressure. Eventually the pressure exceeds the strength of the plug, which fails in stick-slip motion and the pressure is relieved. The magma sticks again when the pressure falls below the dynamic friction value. In this model the time scale of the cycles is controlled by gas diffusion. The influence of permeable gas loss, crystallization and elastic expansion of the conduit on the period of pulsations was studied.

A shorter timescale of order of minutes was investigated in Iverson et al. [43] in relation to repetitive seismic events during the 2004–2006 eruption of Mount St. Helens. The flow dynamics is controlled by the presence of a solid plug that is pushed by a Newtonian liquid, with the possibility of a stick-slip transition. Inertia of the plug becomes important on such short timescales.

Models to explain the occurrence of Vulcanian explosions have also been developed by Connor et al. [15], Jaquet et al. [44] and Clarke et al. [13]. A statistical model of repose periods between explosions by Connor et al. [15] shows that data fit a log-logistic distribution, consistent with the interaction of two competing processes that decrease and increase gas pressure respectively. Jaquet et al. [44] show the explosion repose period data have a memory. The petrological observations of Clarke et al. [13] on clasts from Vulcanian explosions associated with short-term cycles support a model where pressure

524  
525  
526  
527  
528  
529  
530  
531  
532  
533  
534  
535  
536  
537  
538  
539  
540  
541  
542  
543  
544  
545  
546  
547  
548  
549  
550  
551  
552  
553  
554  
555  
556  
557  
558  
559  
560  
561  
562  
563  
564  
565  
566  
567  
568  
569  
570  
571  
572  
573  
574

575 builds up beneath a plug by gas diffusion, but is opposed by  
576 gas leakage through a permeable magma foam. Although  
577 these models include some of the key processes and have  
578 promising explanatory power, they do not consider the de-  
579 velopment of the magma plug explicitly. This process is  
580 considered in [24], where a model of magma ascent with  
581 gas escape is proposed.

### 582 Long-Term Cycles

583 Figure 3 shows views of three lava domes (Mount St. He-  
584 lens, USA, Santiaguito, Guatemala and Shiveluch, Rus-  
585 sia). Measurements of magma discharge rate variations  
586 with time are presented below [25,35,89]. Behavior at the  
587 first two volcanoes is rather regular, whereas at Shiveluch,  
588 long repose periods are followed by an initial rapid in-  
589 crease in eruptive activity with subsequent decrease and  
590 complete stop of the eruption. Growth of the lava dome  
591 at Unzen volcano, Japan, 1991–1995 was similar to Shiv-  
592 eluch [25,68].

593 There are three types of conceptual models that at-  
594 tempt to explain long term variation in magma discharge  
595 rate. Maeda [53], after [42], considers a simple system  
596 that contains a spherical magma chamber located in elas-  
597 tic rocks with a cylindrical conduit located in visco-elas-  
598 tic rocks. Magma viscosity is assumed to be constant. The  
599 magma chamber is replenished with a time dependent in-  
600 flux rate. The model reproduces discharge rate variation  
601 at Unzen volcano by assuming a bell-shaped form of in-  
602 flux rate dependence on time. There are two controver-  
603 sial assumptions in the model. First, the assumption that  
604 the conduit wallrocks are visco-elastic, while the magma  
605 chamber wallrocks are purely elastic cannot be justified  
606 because near the chamber rock temperature is the high-  
607 est and it is more reasonable to expect viscous properties  
608 for chamber wallrocks rather than for the conduit. The  
609 equation that links conduit diameter with magmatic over-  
610 pressure assumes viscous rock properties up to infinity. If  
611 the chamber is located in visco-elastic rocks, oscillations in  
612 discharge rate are not possible. Second, in order to obtain  
613 reasonable timescales, the rock viscosity must be rather  
614 small, of order of  $10^{13}$  Pa s, which is only slightly higher  
615 than the typical viscosities of the magma.

616 Another set of models attribute cyclic behavior to heat  
617 exchange between ascending magma and wallrocks, which  
618 accounts for temperature dependent viscosity [17,95]. The  
619 idea of both models is that magma cools down as it as-  
620 cends, and heat flux is proportional to the difference be-  
621 tween the average temperature of the magma and the  
622 temperature of the wallrocks. If magma ascends quickly  
623 than heat loss is small in comparison with heat advection.

624 Magma viscosity remains low as a consequence and allows  
625 high magma discharge rates. In contrast, when magma  
626 ascends slowly it can cool substantially and viscosity in-  
627 creases significantly. Both models suggest that, for a fixed  
628 chamber pressure, there can be up to three steady state  
629 solutions with markedly different discharge rates. Tran-  
630 sition between these steady-state solutions leads to cyclic  
631 variations in discharge rate. Whitehead and Helfrich [95]  
632 demonstrated the existence of cyclic regimes in exper-  
633 iments using corn syrup. In application to magma as-  
634 cent in a volcanic conduit, these models have strong lim-  
635 itations, because a constant wall-rock temperature is as-  
636 sumed. However, as an eruption progresses the wallrocks  
637 heat up and heat flux decreases, a condition that makes  
638 periodic behavior impossible for long-lived eruptions. For  
639 such a long-lived eruption like Santiaguito (started in  
640 1922) wallrocks are expected to be nearly equilibrated in  
641 temperature with the magma, and heat losses from magma  
642 became small. It is possible that this decrease in heat flux  
643 contributes to a slow progressive increase in temperature  
644 that is observed on timescales longer than the period of  
645 pulsations. For example, magma at Santiaguito becomes  
646 progressively less viscous, resulting in a transition from  
647 mainly lava dome to lava flow activity.

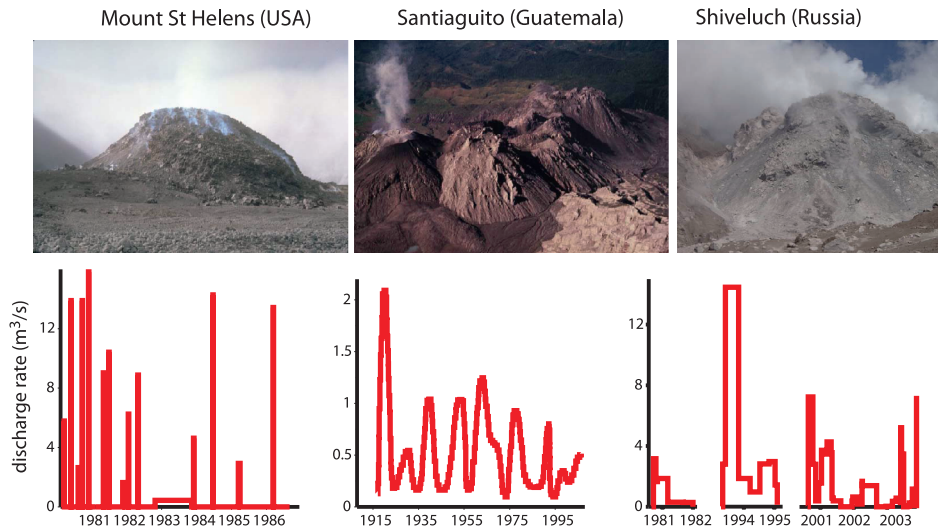
648 Models, developed by authors of this manuscript, con-  
649 sider that degassing-induced crystallization is a major con-  
650 trolling process for the long-term cyclicity during lava  
651 dome building eruptions. There is increasing evidence  
652 that there is a good correlation between magma discharge  
653 rate and crystallinity of the magma [10,68]. An increase  
654 in crystal content leads to an increase in magma viscos-  
655 ity [16,20,21] and, thus, influences magma ascent dynam-  
656 ics. First, we consider a simplified model of magma ascent  
657 in a volcanic conduit that accounts for crystallization and  
658 rheological stiffening.

### A Simplified Model

659 In Barmin et al. [3] the following simplifying assumptions  
660 have been made in order to develop a semi-analytical ap-  
661 proach to magma ascent dynamics.  
662

- 663 1. Magma is incompressible. The density change due to  
664 bubble formation and melt crystallization is neglected.
- 665 2. Magma is a viscous Newtonian fluid. Viscosity is a step  
666 function of crystal content. When the concentration of  
667 crystals  $\beta$  reaches a critical value  $\beta_*$  the viscosity of  
668 magma increases from value  $\mu_1$  to a higher value  $\mu_2$ .  
669 Later on we will consider magma rheology in more de-  
670 tail (see Sect. “Rheology of Crystal-Bearing Magma and  
671 Conduit Resistance”), but a sharp increase in viscosity





**Volcanic Eruptions: Cyclicity during Lava Dome Growth, Figure 3**

Observed discharge rate versus time for (a) Mount St.Helens dome growth and (b) Santiaguito volcano and Shiveluch (c). Photos: Mount St.Helens by Lyn Topinka (1985), Santiaguito by Gregg Bluth (2002), Shiveluch by Pavel Plechov (2001)

- 672 over a narrow range of crystal content has been con-  
 673 firmed experimentally (e. g., [9,48]).
- 674 3. Crystal growth rate is constant and no nucleation oc-  
 675 curs in the conduit. The model neglects the fact that  
 676 magma is a complicated multi-component system and  
 677 its crystallization is controlled by the degree of under-  
 678 cooling (defined as the difference between actual tem-  
 679 perature of the magma and its liquidus temperature).  
 680 Later in the paper a more elaborate model for magma  
 681 crystallization will be considered.
- 682 4. The conduit is a vertical cylindrical pipe. Elastic defor-  
 683 mation of the wallrocks is not included in the model.  
 684 This assumption is valid for a cylindrical shape of the  
 685 conduit at typical magmatic overpressures, but is vio-  
 686 lated when the conduit has a fracture shape. Real ge-  
 687 ometries of volcanic conduits and their inclination can  
 688 vary significantly with depth.
- 689 5. The magma chamber is located in elastic rocks and is  
 690 fed from below, with a constant influx rate. For some  
 691 volcanoes, like Santiaguito or Mount St.Helens, average  
 692 magma discharge rate remained approximately constant  
 693 during several periods of pulsation. Thus the assump-  
 694 tion of constant influx rate is valid. For volcanoes  
 695 like Mount Unzen or Shiveluch, there is an evidence of  
 696 pulse-like magma recharge [25,53].

697 With above simplification the system of equations for un-  
 698 steady 1D flow is as follows:

$$699 \frac{\partial}{\partial t} \rho + \frac{\partial}{\partial x} \rho u = 0; \quad \frac{\partial}{\partial t} n + \frac{\partial}{\partial x} n u = 0 \quad (1a)$$

$$700 \frac{\partial p}{\partial x} = -\rho g - \frac{32\mu u}{\delta^2}; \quad \mu = \begin{cases} \mu_1, & \beta < \beta_* \\ \mu_2, & \beta \geq \beta_* \end{cases} \quad (1b)$$

$$701 \frac{\partial}{\partial t} \beta + u \frac{\partial \beta}{\partial x} = 4\pi n r^2 \chi = (36\pi n)^{\frac{1}{3}} \beta^{\frac{2}{3}} \chi \quad (1c)$$

702 Here  $\rho$  is the density of magma,  $u$  is the vertical cross-sec-  
 703 tion averaged ascent velocity,  $n$  is the number density of  
 704 crystals per unit volume,  $p$  is the pressure,  $g$  is the accel-  
 705 eration due to gravity,  $\delta$  is the conduit diameter,  $\beta$  is the  
 706 volume concentration of crystals,  $\beta_*$  is a critical concen-  
 707 tration of crystals above which the viscosity changes from  
 708  $\mu_1$  to  $\mu_2$ ,  $r$  is the crystal radii,  $\chi$  is the linear crystal growth  
 709 rate, and  $x$  is the vertical coordinate. The first two Eqs. (1a)  
 710 represent the conservation of mass and the number den-  
 711 sity of crystals, the second (1b) is the momentum equa-  
 712 tion with negligible inertia, and the third (1c) is the crystal  
 713 growth equations with  $\chi = \text{constant}$ . We assume the fol-  
 714 lowing boundary conditions for the system (1):

$$715 x = 0 : \frac{dp_{ch}}{dt} = \frac{\gamma}{V_{ch}} (Q_{in} - Q_{out}); \quad \beta = \beta_{ch}; \quad n = n_{ch}$$

$$x = l : p = 0$$

716 Here  $\gamma$  is the rigidity of the wall-rock of the magma cham-  
 717 ber,  $V_{ch}$  is the chamber volume,  $\beta_{ch}$  and  $n_{ch}$  are the crystal  
 718 concentration and number density of crystals per unit vol-  
 719 ume in the chamber,  $p_{ch}$  is the pressure in the chamber,  $l$   
 720 is the conduit length,  $Q_{in}$  is the flux into the chamber and  
 721  $Q_{out} = \pi \delta^2 u / 4$  is the flux out of the chamber into the  
 722 conduit. Both  $\beta_{ch}$  and  $n_{ch}$  are assumed constant. We neglect

723 the influence of variations of the height of the lava dome  
724 on the pressure at the top of the conduit and assume that  
725 the pressure there is constant. As the magma is assumed  
726 to be incompressible, the pressure at the top of the con-  
727 duit can be set to zero because the atmospheric pressure is  
728 much smaller than magma chamber pressure.

729 From the mass conservation equation for the case of  
730 constant magma density,  $u = u(t)$  and  $n = n_{\text{ch}}$  every-  
731 where. Equations (1) can be integrated and transformed  
732 from partial differential equations to a set of ordinary dif-  
733 ferential equations with state-dependent delay represent-  
734 ing a “memory” effect on crystal concentration (see [3] for  
735 details).

### 736 Results and Applications

737 The general steady-state solution for magma ascent veloc-  
738 ity variations with chamber pressure is shown in Fig. 4a.  
739 Solutions at high magma ascent velocities, when the criti-  
740 cal concentration of crystals is not reached inside the con-  
741 duit, result in a straight line (CB), which is the same as for  
742 the classical Poiseuille solution for a fluid with constant  
743 viscosity. At low ascent velocities there is a quadratic re-  
744 lationship (OAC) between chamber pressure and ascent  
745 velocity (see [3] for derivation of the equation). A key fea-  
746 ture of the steady-state solution is that, for a fixed cham-  
747 ber pressure, it is possible to have three different magma  
748 ascent velocities. We note that for  $\mu_2/\mu_1 = 1$  only the  
749 branch CB exists and for  $1 < \mu_2/\mu_1 \leq 2$  there is a smooth  
750 transition between the lower branch (ODA) and the up-  
751 per branch (CB) and multiple steady-state regimes do not  
752 exist.

753 We first consider the case where chamber pressure  
754 changes quasi-statically and the value of  $Q_{\text{in}}$  is between  
755  $Q_A$  and  $Q_C$ . Starting at point O the chamber pressure in-  
756 creases, because the influx into the chamber is higher than  
757 the outflux. At point A, a further increase in pressure is not  
758 possible along the same branch of the steady-state solution  
759 and the system must change to point B, where the outflux  
760 of magma is larger than the influx. The chamber pressure  
761 and ascent velocity decrease along BC until the point C is  
762 reached and the system must change to point D. The cycle  
763 DABC then repeats itself. Provided the chamber continues  
764 to be supplied at the same constant rate repetition of this  
765 cycle results in periodic behavior. The transitions AB and  
766 CD in a cycle must involve unsteady flow.

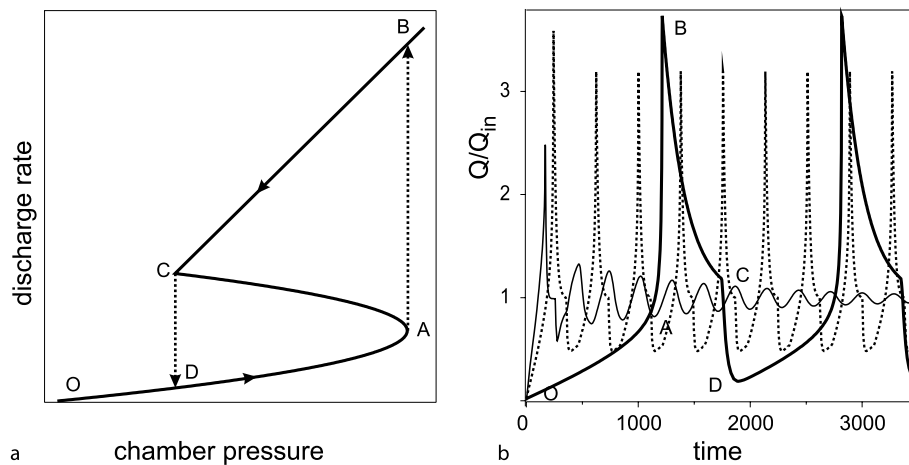
767 Oscillations in magma discharge rate involve large  
768 variations in magma crystal content. This relation is ob-  
769 served on many volcanoes. For example, pumice and sam-  
770 ples of the Soufrière Hills dome that were erupted during  
771 periods of high discharge [88] have high glass contents (25

772 to 35%) and few microlites [65], whereas samples derived  
773 from parts of the dome that were extruded more slowly  
774 (days to weeks typically) have much lower glass contents  
775 (5 to 15%) and high contents of groundmass microlites.  
776 These and other observations [34,68] suggest that micro-  
777 lite crystallization can take place on similar time scales to  
778 the ascent time of the magma.

779 Of more general interest is to consider unsteady flow  
780 behaviour. We assume that the initial distribution of param-  
781 eters in the conduit corresponds to the steady-state solu-  
782 tion of system (1) with the initial magma discharge rate,  
783  $Q_0$ , being in the lowest regime. The behaviour of an erup-  
784 tion with time depends strongly on the value of  $Q_{\text{in}}$ . If  
785  $Q_{\text{in}}$  corresponds to the upper or the lower branch of the  
786 steady state solution the eruption stabilizes with time with  
787  $Q = Q_{\text{in}}$  and  $dp_{\text{ch}}/dt = 0$ . However, if  $Q_{\text{in}}$  corresponds  
788 to the intermediate branch of the steady-state solution,  
789 with  $Q_{\text{in}}$  between  $Q_A$  and  $Q_C$ , periodic behaviour is pos-  
790 sible. Figure 4b shows three eruption scenarios for differ-  
791 ent values of the magma chamber volume  $V_{\text{ch}}$ . When  $V_{\text{ch}}$   
792 is small the eruption stabilizes with time. In contrast, un-  
793 damped periodic oscillations occur for values of  $V_{\text{ch}}$  larger  
794 than some critical value. For very large magma chamber  
795 volumes the transient solution almost exactly follows the  
796 steady-state solution, with unsteady transitions between  
797 the regimes. The time that the system spends in unsteady  
798 transitions in this case is much shorter than the period of  
799 pulsations. The maximum discharge rate during the cycle  
800 is close to  $Q_B$ , the minimum is close to  $Q_D$  and the average  
801 is equal to  $Q_{\text{in}}$ . The period of pulsations increases as the  
802 volume of magma chamber increases.

803 Now we apply the model to two well-documented  
804 eruptions: the growth of lava domes on Mount St. Helens  
805 (1980–1986) and on Santiaguito (1922–present). Our  
806 objective here is to establish that the model can repro-  
807 duce the periodic behaviors observed at these two volca-  
808 noes. Estimates can be obtained for most of the system pa-  
809 rameters. However, magma chamber size is not well-con-  
810 strained and so the model can be used to make qualitative  
811 inferences on relative chamber size. Given the uncertain-  
812 ties in the parameter values and the simplifications in the  
813 model development, the approach can be characterized as  
814 mimicry. Adjustments in some parameters were made to  
815 achieve best fits with observations, but the particular best-  
816 fits are not unique.

817 For Mount St. Helens our model is based on data  
818 presented by [89]. Three periods of activity can be dis-  
819 tinguished during the period of dome growth. The first  
820 period consists of 9 pulses of activity with average peak  
821 magma discharge rates  $\sim 15 \text{ m}^3/\text{s}$  during 1981–1982. Each  
822 pulse lasted from 2 to 7 days (with a mean value of 4 days)



**Volcanic Eruptions: Cyclicity during Lava Dome Growth, Figure 4**

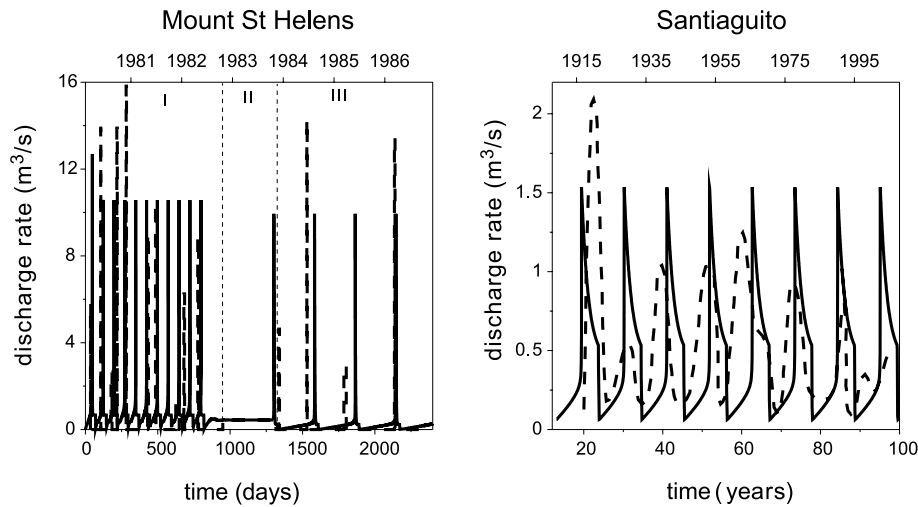
The general steady-state solution and possible quasi-static evolution of an eruption. After [3]. Different curves correspond to different values of dimensionless parameter  $\kappa = (\pi \delta^2 \gamma) / (4V_{ch} \rho g)$  (0.12 – thin line, 0.05 – dotted line, and 0.005 – bold line)

823 with the average period between the pulses being 74 days  
 824 and the average discharge rate during the period being  
 825  $Q_1 \sim 0.67 \text{ m}^3/\text{s}$ . The second period is represented by  
 826 continuous dome growth and lasted more than a year (368  
 827 days) with a mean magma discharge rate of  $Q_2 \sim 0.48$   
 828  $\text{m}^3/\text{s}$ . During the last period there were 5 episodes of dome  
 829 growth with peak magma discharge rates up to  $\sim 15 \text{ m}^3/\text{s}$ ,  
 830 an average period of pulsation of  $\sim 230$  days and a mean  
 831 discharge rate of  $Q_3 \sim 0.23 \text{ m}^3/\text{s}$ . We assume that the in-  
 832 tensity of influx into the magma chamber,  $Q_{in}$ , is equal to  
 833 the average magma discharge rate over the corresponding  
 834 periods. There might have been a progressive decrease in  
 835 the intensity of influx during the eruption, but, due to lim-  
 836 itations of the model, we assume that  $Q_{in}$  changes as a step  
 837 function between the periods.

838 The best-fit model for the eruption is presented in  
 839 Fig. 5a, with the parameters used for the simulation sum-  
 840 marized in Table 2 in [3]. During the first period of the  
 841 eruption  $Q_{in} = Q_1$ . This corresponds to the intermediate  
 842 branch of the steady-state solution and cyclic behaviour  
 843 occurs. In the second period  $Q_{in} = Q_2$  the system moves  
 844 to the lower regime and the eruption stabilizes with time.  
 845 For the third period of the eruption the parameters of the  
 846 system have been changed, so that  $Q_{in} = Q_3 < Q_2$ , cor-  
 847 responding to the intermediate regime once again and peri-  
 848 odic behaviour occurs. This condition can be satisfied by  
 849 a decrease in the diameter of the conduit, or a decrease  
 850 in crystal growth rate, or the number density of crystals.  
 851 All these mechanisms are possible: decrease in the diam-  
 852 eter could be a consequence of magma crystallization on  
 853 the conduit walls, while a decrease in either crystal growth

rate or number density of crystals could be reflect ob-  
 854 served changes in magma composition [89]. The influence  
 855 of conduit diameter is the strongest because ascent veloc-  
 856 ity, for the same discharge rate, depends on the square  
 857 of the diameter. The required change in diameter is from  
 858 18 to 12 m, but this change can be smaller if we assume  
 859 a simultaneous decrease in crystal growth rate.

860 Since 1922, lava extrusion at Santiaguito has been  
 861 cyclic [35]. Each cycle begins with a 3–6 year long high  
 862 (0.5–2.1  $\text{m}^3/\text{s}$ ) magma discharge rate phase, followed by  
 863 a longer (3–11 years) low ( $\sim 0.2 \text{ m}^3/\text{s}$ ) discharge rate  
 864 phase. The time-averaged magma discharge rate was al-  
 865 most constant at  $\sim 0.44 \text{ m}^3/\text{s}$  between 1922 and 2000. The  
 866 first peak in discharge rate had a value  $> 2 \text{ m}^3/\text{s}$ , whereas  
 867 the second peak had a much smaller value. The value for  
 868 the second peak is underestimated as it is calculated based  
 869 on the dome volume only, but does not include the volume  
 870 of dome collapse pyroclastic flows. Later peaks show an in-  
 871 crease in magma discharge rate until 1960 (Fig. 5b, dashed  
 872 line). Post-1960, the duration of the low discharge rate  
 873 phase increased, the peak discharge and the time-averaged  
 874 discharge rates for each cycle decreased, and the difference  
 875 between discharge rates during the high and low discharge  
 876 rate phases of each cycle decreased. Our best-fit model is  
 877 shown in Fig. 5b and the parameters estimates are listed  
 878 in Table 2 in [3]. The model reproduces the main features  
 879 of the eruption, including the period of pulsations, the ra-  
 880 tio between low and high magma discharge rates, and the  
 881 range of observed discharge rates. We cannot, however, re-  
 882 produce the decrease in the amplitude of pulsations within  
 883 the framework of the model using fixed parameter values.  
 884



Volcanic Eruptions: Cyclicity during Lava Dome Growth, Figure 5

Discharge rate versus time for a Mount St.Helens dome growth and b Santiaguito volcano. Dotted lines represent are the observed values of discharge rates and the solid lines are the best fit simulations. After [3]

885 The theory provides a potential method to estimate  
 886 magma chamber volumes. For Mount St.Helens our estimate  
 887 of the chamber size ( $\sim 0.6 \text{ km}^3$ ) is comparable with  
 888 the total erupted volume in the entire 1980–1986 eruption  
 889 and is consistent with the fact that geophysical imaging  
 890 did not identify a large magma body. Santiaguito volcano  
 891 erupted more than  $10 \text{ km}^3$  in the 1902 explosive eruption  
 892 [96] and more than  $1 \text{ km}^3$  of lava domes since 1922.  
 893 The best-fit model estimate of a large ( $64 \text{ km}^3$ ) chamber  
 894 is consistent with much larger eruption volumes, long periods,  
 895 and longevity of the eruption in comparison to Mount  
 896 St. Helens. One limitation of the model is that the supply  
 897 of deep magma from depth to the chamber is assumed to  
 898 be constant.

### 899 Model Development

900 In this section we further develop models to examine new  
 901 effects and relax some of the simplifications of earlier  
 902 models. We investigate a number of effects that were not  
 903 fully explained or considered in previous studies [3,61,62].  
 904 The new model incorporates a more advanced treatment  
 905 of crystallization kinetics based on the theoretical concepts  
 906 developed in [38,46], and is calibrated by experimental  
 907 studies in andesitic systems [22,34]. In particular, we  
 908 distinguish growth of phenocrysts formed in the magma  
 909 chamber from crystallization of microlites during magma  
 910 ascent. Previous models have assumed that magma is always  
 911 Newtonian, so we study models of conduit flow assuming  
 912 non-Newtonian rheology, with rheological prop-

erties being related to crystal content. Latent heat is re-  
 913 leased during the crystallization of ascending magma due  
 914 to degassing and we show that this can have an important  
 915 influence on the dynamics. Elastic deformation of conduit  
 916 walls leads to coupling between magma ascent and vol-  
 917 cano deformations.  
 918

**System of Equations** We model magma ascent in  
 919 a dyke-shaped conduit with elliptical cross-section using  
 920 a set of 1D transient equations written for horizontally averaged  
 921 variables [20,21]:  
 922

$$\frac{1}{S} \frac{\partial}{\partial t}(S\rho_m) + \frac{1}{S} \frac{\partial}{\partial x}(S\rho_m V) = -G_{mc} - G_{ph} \quad (2) \quad 923$$

$$\frac{1}{S} \frac{\partial}{\partial t}(S\rho_{mc}) + \frac{1}{S} \frac{\partial}{\partial x}(S\rho_{mc} V) = G_{mc} \quad (3a) \quad 924$$

$$\frac{1}{S} \frac{\partial}{\partial t}(S\rho_{ph}) + \frac{1}{S} \frac{\partial}{\partial x}(S\rho_{ph} V) = G_{ph} \quad (3b) \quad 925$$

$$\frac{1}{S} \frac{\partial}{\partial t}(S\rho_d) + \frac{1}{S} \frac{\partial}{\partial x}(S\rho_d V) = -J \quad (4a) \quad 926$$

$$\frac{1}{S} \frac{\partial}{\partial t}(S\rho_g) + \frac{1}{S} \frac{\partial}{\partial x}(S\rho_g V_g) = J \quad (4b) \quad 927$$

928 Here  $t$  denotes time,  $x$  the vertical coordinate,  $\rho_m, \rho_{ph}, \rho_{mc},$   
 929  $\rho_d$  and  $\rho_g$  are the densities of melt, phenocrysts, microlites,  
 930 dissolved gas and exsolved gas respectively, and  $V$  and  $V_g$   
 931 are the velocities of magma and gas, respectively.  $G_{ph}, G_{mc}$   
 932 represent the mass transfer rate due to crystallization of  
 933 phenocrysts and microlites, respectively, and  $J$  the mass  
 934 transfer rate due to gas exsolution,  $S$  is the cross-section



935 area of the conduit. Equation (2) represents the mass con-  
936 servation for the melt phase, Eqs. (3a) and (3b) are the con-  
937 servation equations for microlites and phenocrysts respec-  
938 tively, Eqs. (4a) and (4b) represent the conservation of the  
939 dissolved gas and of the exsolved gas respectively.

$$940 \quad \frac{\partial p}{\partial x} = -\rho g - F_c \quad (5)$$

$$941 \quad V_g - V = -\frac{k}{\mu_g} \frac{\partial p}{\partial x} \quad (6)$$

942 Here  $p$  is the pressure,  $\rho$  the bulk density of magma,  $g$  the  
943 acceleration due to gravity,  $\mu$  is the magma viscosity,  $k$  is  
944 the magma permeability and  $\mu_g$  is the gas viscosity. Eq. (5)  
945 represents the equation of momentum for the mixture as  
946 a whole, in which the pressure drops due to gravity and  
947 conduit resistance are calculated for laminar flow in an el-  
948 liptic pipe. Equation (6) is the Darcy law for the exsolved  
949 gas flux through the magma.

$$950 \quad \frac{1}{S} \frac{\partial}{\partial t} (S\rho C_m T) + \frac{1}{S} \frac{\partial}{\partial x} (S\rho C_m VT) \\ 951 \quad = L_*(G_{mc} + G_{ph}) - C_m TJ - Q_{cl} + Q_{vh} \quad (7)$$

954 Here  $C_m$  is the bulk specific heat of magma,  $T$  is the bulk  
955 flow-averaged temperature,  $L_*$  is latent heat of crystal-  
956 lization,  $Q_{cl}$  denotes the total heat loss by conduction to  
957 the conduit walls, and  $Q_{vh}$  denotes the total heat genera-  
958 tion due to viscous dissipation. Here we consider the case  
959 of the latent heat release. This assumption is valid when  
960 both  $Q_{cl} \approx 0$  and  $Q_{vh} \approx 0$  or when  $Q_{cl} + Q_{vh} \approx 0$ . The  
961 study of the effects of both heat loss and viscous heating,  
962 which are intrinsically two-dimensional [18,19], and their  
963 parametrization is the subject of ongoing research.

$$964 \quad \rho_m = \rho_m^0(1-\alpha)(1-\beta)(1-c); \quad \rho_c = \rho_c^0(1-\alpha)\beta \quad (8a)$$

$$965 \quad \rho_d = \rho_m^0(1-\alpha)(1-\beta)c; \quad \rho_g = \rho_g^0\alpha \quad (8b)$$

$$966 \quad \rho = \rho_m + \rho_c + \rho_d + \rho_g \quad (8c)$$

$$967 \quad \alpha = \frac{4}{3}\pi r_b^3 n; \quad \frac{\partial}{\partial t}(Sn) + \frac{\partial}{\partial x}(SnV) = 0; \quad p = \rho_g^0 RT \quad (9)$$

968 Here  $\alpha$  is the volume concentration of bubble,  $\beta$  is the  
969 volume concentration of crystals in the condensed phase  
970 (melt plus crystals), and  $c$  is mass concentration of dis-  
971 solved gas (equal to volume concentration as we assume  
972 that the density of dissolved volatiles is the same as the  
973 density of the melt),  $\rho_0^m$  denotes the mean density of the  
974 pure melt phase,  $\rho_0^c$  is density of the pure crystal phase  
975 (with  $\rho_c = \rho_{ph} + \rho_{mc}$ ,  $\beta = \beta_{ph} + \beta_{mc}$ ),  $r_b$  is the bubble

976 radius, and  $n$  the number density of bubble per unit vol-  
977 ume. Concerning the parametrization of mass transfer rate  
978 functions, we use:

$$979 \quad J = 4\pi r_b n D \rho_m^0 (c - C_f \sqrt{p}) \quad (10)$$

$$980 \quad G_{mc} = 4\pi \rho_c^0 (1-\beta)(1-\alpha) \\ 981 \quad \times U(t) \int_0^t I(\omega) \left( \int_0^t U(\eta) d\eta \right)^2 d\omega \quad (11a)$$

$$982 \quad G_{ph} = 3\gamma_s \left( \frac{4\pi N_{ph} \beta_{ph}^2}{3} \right)^{\frac{1}{3}} \rho_c^0 (1-\beta)(1-\alpha) U(t) \quad (11b)$$

982 Here  $J$  is parametrized using the analytical solution de-  
983 scribed in [69],  $U$  is the linear crystal growth rate ( $m s^{-1}$ ),  
984  $I$  is the nucleation rate ( $m^{-3} s^{-1}$ ), which defines the num-  
985 ber of newly nucleated crystal per cubic meter, and  $\gamma_s$   
986 is a shape factor of the order of unity,  $D$  and  $C_f$  are  
987 the diffusion and the solubility coefficients, respectively.  
988 Concerning the mass transfer due to crystallization  $G_{mc}$ ,  
989 we adapt a model similar to that described in [38]. As-  
990 suming spherical crystals, the Avrami–Johnson–Mehl–  
991 Kolmogorov equation in the form adopted by [46], for the  
992 crystal volume increase rate, is:

$$993 \quad \frac{d\beta}{dt} = 4\pi Y_t U(t) \int_0^t I(\omega) \left( \int_0^t U(\eta) d\eta \right)^2 d\omega$$

994 where  $Y_t = (1-\beta)(1-\alpha)$  is the volume fraction of melt  
995 remaining uncrystallized at the time  $t$ . Therefore, we have  
996  $G_{mc} = \rho_{mc} d\beta/dt$ . For the phenocryst growth rate ( $\cdot$ ) we  
997 assume that it is proportional to the phenocryst volume  
998 increase rate  $d\beta_{ph}/dt = 4\pi R_{ph}^2 N_{ph} U(t)$  times the crystal  
999 density  $\rho_c^0$  times the volume fraction of melt remaining  
1000 uncrystallized at the time  $t$ . A detailed description of the  
1001 parametrization used for the different terms is reported  
1002 in [63].

1003 For parametrizations of magma permeability  $k$  and  
1004 magma viscosity  $\mu$  we use:

$$1005 \quad k = k(\alpha) = k_0 \alpha^j \quad (12)$$

$$1006 \quad \mu = \mu_m(c, T) \theta(\beta) \eta(\alpha, Ca) \quad (13)$$

1007 where  $k$  is assumed to depend only on bubble volume  
1008 fraction  $\alpha$ . Magma viscosity  $\mu$  depends on water content,  
1009 temperature, crystal content, bubble fraction and capillary  
1010 number as described in detail in the next section.

1011 Regarding equations for semi-axes,  $a$  and  $b$ , we assume  
1012 that the elliptical shape is maintained and that pressure  
1013 change gradually in respect with vertical coordinate and

1014 time so that the plain strain analytical solution for an ellipse  
1015 subjected to a constant internal overpressure [64,66],  
1016 remains valid:

$$1017 \quad a = a_0 + \frac{\Delta P}{2G} [-(1 - 2\nu)a_0 + 2(1 - \nu)b_0] \quad (14a)$$

$$1018 \quad b = b_0 + \frac{\Delta P}{2G} [2(1 - \nu)a_0 - (1 - 2\nu)b_0] \quad (14b)$$

1019 where  $\Delta P$  is the overpressure, i. e. the difference between  
1020 conduit pressure and far field pressure (here assumed to be  
1021 lithostatic for a sake of simplicity),  $a_0$  and  $b_0$  are the initial  
1022 values of the semi-axes,  $\nu$  is the host rock Poisson ratio,  
1023 and  $G$  is the host rock rigidity.

1024 Equations (2)–(14) are solved between the top of  
1025 the magma chamber and the bottom of the lava dome  
1026 that provides some constant load by using the numerical  
1027 method described in [63]. The effects of dome height  
1028 and morphology changes are not considered in this paper.  
1029 We consider three different kinds of boundary conditions  
1030 at the inlet of the dyke: constant pressure, constant  
1031 influx rate and the presence of a magma chamber located  
1032 in elastic rocks. The case of constant pressure is applica-  
1033 ble when a dyke starts from either a large magma chamber  
1034 or unspecified source, so that pressure variations in the  
1035 source region remain small. An estimate of the volume of  
1036 magma stored in the source region that allows pressure to  
1037 be approximated as constant depends on wall-rock elasticity,  
1038 magma compressibility (volatile content), and the total  
1039 volume of the erupted material. If the magma flow at depth  
1040 is controlled by regional tectonics, the case of constant  
1041 influx rate into the dyke may be applicable if total variations  
1042 in supply rate are relatively small on the timescale of the  
1043 eruption.

1044 For the case where magma is stored in a shallow  
1045 magma chamber prior to eruption, and significant chamber  
1046 replenishment occurs, the flow inside the conduit must  
1047 be coupled with the model for the magma chamber. In this  
1048 case, as explained in detail in [63], we assume that the  
1049 relationship between the pressure at the top of the magma  
1050 chamber  $p_{ch}$  and the intensity of influx  $Q_{in}$  and outflux  
1051  $Q_{out}$  of magma to and from the chamber is given by:

$$1052 \quad \frac{dp_{ch}}{dt} = \frac{4G \langle K \rangle}{\langle \rho \rangle V_{ch} (3 \langle K \rangle + 4G)} (Q_{in} - Q_{out}) \quad (15)$$

1053 where  $V_{ch}$  is the magma chamber volume,  $\langle \rho \rangle$  and  $\langle K \rangle$  are  
1054 the average magma density and magma bulk modulus, respec-  
1055 tively, and  $G$  is the rigidity of rocks surrounding the  
1056 chamber.

1057 Cases of constant influx and of constant source pres-  
1058 sure are the limit cases of Eq. (15) in the case of infinitely

1059 small and infinitely large magma chamber volume. We as-  
1060 sume that the volume concentration of bubbles and phenocrysts  
1061 are determined by equilibrium conditions and that the tempera-  
1062 ture of the magma is constant. The effect of temperature change  
1063 on eruption dynamics, due to interaction between silicic and  
1064 basaltic magma, was studied in [63].

1065 We use a steady-state distribution of parameters along  
1066 the conduit as an initial condition for the transient simulation.  
1067 The values are calculated for a low magma discharge rate, but  
1068 the particular value of this parameter is not important because  
1069 the system deviates from initial conditions to a cyclic or  
1070 stabilized state, which does not depend on the initial conditions.  
1071

### 1072 Rheology of Crystal-Bearing Magma and Conduit Resistance

1073 Magma viscosity is modeled as a product of melt  
1074 viscosity  $\mu_m(c, T)$ , the relative viscosity due to crystal  
1075 content  $\theta(\beta) = \Theta(\beta)\varphi(\beta)$ , and the relative viscosity due  
1076 to the presence of bubbles  $\eta(\alpha, Ca)$ . The viscosity of the  
1077 pure melt  $\mu_m(c, T)$  is calculated according to [36]. Viscosity  
1078 increase due to the presence of the crystals is described  
1079 through the function  $\Theta(\beta)$  [16,20,21]. As crystallization  
1080 proceeds, the remaining melt becomes enriched in silica-  
1081 and melt viscosity increases. The parametrization of this  
1082 effect is described by the function  $\varphi(\beta)$  in [21,25]. Effects  
1083 of the solid fraction are parametrized as described in [21].

1084 Effects due to the presence of bubbles are accounted  
1085 for by adopting a generalization of [51] for an elliptical  
1086 conduit [20,21].

1087 In the case of Newtonian magma rheology, the friction  
1088 force in an elliptical conduit can be obtained from a  
1089 classical Poiseuille solution for low Reynolds number  
1090 flow  $F_c = 4\mu(a^2 + b^2)/(a^2b^2)V$  [47]. High crystal or  
1091 bubble content magmas may show non-Newtonian rheology.  
1092 One possible non-Newtonian rheology is that of a Bingham  
1093 material characterized by a yield strength  $\tau_b$  [4]. The  
1094 stress-strain relation for this material is given by:  
1095

$$1096 \quad \begin{aligned} \tau_{ij} &= \left( \mu + \frac{\tau_b}{\gamma} \right) \gamma_{ij} \Leftrightarrow \tau > \tau_b \\ \gamma_{ij} &= 0 \Leftrightarrow \tau \leq \tau_b \end{aligned} \quad (16)$$

1097 Here  $\tau_{ij}$  and  $\gamma_{ij}$  are the stress and strain rate tensors,  $\tau$  and  
1098  $\gamma$  are second invariants of corresponding tensors. Accord-  
1099 ing to this rheological law, the material behaves linearly  
1100 when the applied stress is higher than a yield strength. No  
1101 motion occurs if the stress is lower than a yield strength.  
1102 In the case of a cylindrical conduit the average velocity  
1103 can be calculated in terms of the stress on the conduit wall

1104  $\tau_w$  [52]:

$$1105 \quad V = \frac{1}{12} \frac{r}{\tau_w^3 \mu} (\tau_b^4 + 3\tau_w^4 - 4\tau_b \tau_w^3) \quad (17)$$

1106 Here  $r$  is the conduit radii. This form of equation gives  
1107 an implicit relation between ascent velocity and pressure  
1108 drop, and is not convenient to use. By introducing dimensionless  
1109 variables  $\Pi = \mu V / \tau_b r$  and  $\Theta = \tau_w / \tau_b \geq 1$  relation  
1110 (17) can be transformed into:

$$1111 \quad \Theta^4 - \frac{1}{6} (8 + 3\Pi) \Theta^3 + \frac{1}{3} = 0 \quad (18)$$

1112 Following [63] a semi-analytical solution can be used for  
1113 (18) and the conduit friction force can be expressed finally  
1114 as:

$$1115 \quad F_c = \frac{2\tau_w}{r} = \frac{2\tau_b \Theta (\Pi)}{r}.$$

1116 We note that a finite pressure gradient is necessary to initiate  
1117 the flow in the case of Bingham liquid, in contrast to  
1118 a Newtonian liquid.

## 1119 Results and Applications

1120 *Influence of non-Newtonian Properties on Eruption Behaviour*  
1121 Now we compare the dynamics of magma extrusion in the cases of  
1122 Newtonian and Bingham rheology. We will assume that yield strength  
1123 is reached when the concentration of crystals reaches a critical value:  
1124

$$1125 \quad \tau = \begin{cases} \tau_b & \text{for } \beta > \beta_{cr} \\ 0 & \text{for } \beta \leq \beta_{cr} \end{cases} \quad (19)$$

1126 Figure 6a shows a set of steady-state solutions for different  
1127 values of  $\tau_b$ . Values of  $\tau_b$  and  $\beta_{cr}$  depend on crystal shape,  
1128 crystal size distribution, magma temperature and other properties,  
1129 but here are assumed to be constant. To illustrate the influence  
1130 of Bingham rheology, the value of  $\beta_{cr} = 0.65$  was chosen so that,  
1131 for discharge rate larger than  $\sim 5 \text{ m}^3/\text{s}$ , the magma has  
1132 Newtonian rheology (see Fig. 6a). A more detailed study would  
1133 require measurements of the rheological properties of magma for  
1134 a wide range of crystal content and crystal size distributions.  
1135 As the value of  $\tau_b$  the chamber pressure that is necessary to  
1136 start the eruption increases.

1137 Figure 6b shows the influence of these two rheological models  
1138 on the dynamics of magma extrusion. In the case of Bingham  
1139 rheology, magma discharge rate between the two pulses is zero  
1140 until a critical chamber overpressure is reached. Then the magma  
1141 discharge rate increases

1142 rapidly with decrease in crystal content, leading to a significant  
1143 reduction of both magma viscosity and the length of the part of  
1144 the conduit that is occupied by the Bingham liquid where  $\beta_c > \beta_{cr}$ .  
1145 There is a transition in the system to the uppermost flow regime  
1146 and the pressure then decreases quickly. Because the pressure at  
1147 the onset of the pulse was significantly larger than in the case of  
1148 a Newtonian liquid, the resulting discharge rate in the case of  
1149 Bingham rheology is also significantly higher.  
1150  
1151

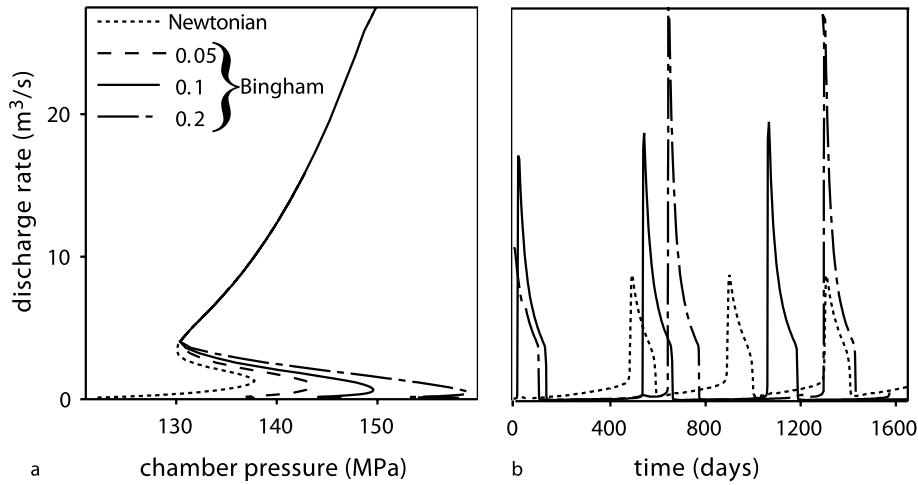
*Modeling of Conduit Flow during Dome Extrusion on Shiveluch Volcano*

1152 The maximum intensity of extrusion was reached at an early stage  
1153 in all three eruptions (Fig. 3). We therefore suggest that dome  
1154 extrusion was initiated by high overpressure in the magma chamber  
1155 with respect to the lithostatic pressure. Depressurization of the  
1156 magma chamber occurred as a result of extrusion. Without magma  
1157 chamber replenishment, depressurization results in a decrease in  
1158 magma discharge rate. In open system chambers replenishment of  
1159 the chamber during eruption can lead to pulsatory behaviour [3].  
1160 The following account is derived from [25]. For the 1980–1981  
1161 eruption the monotonic decrease in discharge rate indicates that  
1162 there was little or no replenishment of the magma chamber.  
1163 During the 1993–1995 and 2001–2004 episodes, however, the  
1164 magma discharge rate fluctuated markedly, suggesting that  
1165 replenishment was occurring. The influx of new magma causes  
1166 an increase in magma chamber pressure, and a subsequent increase  
1167 in magma discharge rate. During the 2001–2004 eruption there  
1168 were at least three peaks in discharge rate. Replenishment of  
1169 the magma chamber with new hot magma can explain the transition  
1170 from lava dome extrusion to viscous lava flow that occurred on  
1171 Shiveluch after 10 May 2004, and which continues at the time  
1172 of writing (2007).  
1173  
1174  
1175  
1176

1177 We simulated dome growth during the 2001–2002, because this  
1178 dataset is the most complete and is supported by petrological  
1179 investigations [39]. We assume the shape of the influx curve:  
1180

$$1181 \quad Q_{in} = \begin{cases} 0, & t < t_s \\ Q_0, & t_s \leq t \leq t_f \\ 0, & t > t_f \end{cases} \quad (20)$$

1182 Influx occurs with constant intensity  $Q_0$  between times  $t_s$   
1183 and  $t_f$ . We have examined many combinations of values of  
1184 these parameters within the constraints provided by observations.  
1185 The best simulation results use the following values of parameters:  
1186  $Q_0 = 3.8 \text{ m}^3/\text{s}$ ,  $t_s = 77$  and  $t_f = 240$  days. A more  
1187 continuous influx, dependent on time, is plausible, but there is  
1188 no geophysical evidence that allows us to



**Volcanic Eruptions: Cyclicity during Lava Dome Growth, Figure 6**

**a** Steady-state solutions and dependence of discharge rate on time for Newtonian and Bingham rheology of the magma. Yield strength is a parameter marked on the curves (values in MPa). For Bingham rheology discharge rate remains zero between the pulses of activity. Bingham rheology results in much higher chamber pressures prior to the onset of activity and, therefore, much higher discharge rates in comparison with Newtonian rheology. **b** Comparison of the period of pulsation in discharge rate for Newtonian and Bingham rheologies. After [63]

1189 constrain the intensity of the influx, because ground deformation  
 1190 data are absent for Shiveluch volcano. The output  
 1191 of the model gives a magma chamber volume of 12 km<sup>3</sup>,  
 1192 assuming a spherical chamber. Figure 7a shows the time-  
 1193 dependence of magma discharge rate, and Fig. 7b shows  
 1194 the increase in the volume of erupted material with time  
 1195 after 6th June 2001. The timing of magma influx is in good  
 1196 agreement with the residence time of basaltic magma in  
 1197 the system, as calculated from the olivine reaction rims.  
 1198 For further details see [25].

1199 *5 to 7 Weeks Cycles on the Soufriere Hills Volcano: Evidence*  
 1200 *for a Dyke?* An approximately 5 to 7 week cyclic pattern  
 1201 of activity was recognized at the Soufrière Hills Volcano  
 1202 (SHV) [87,91] between April 1997 and March 1998 from  
 1203 peaks in the intensity of eruptive activity and geophysical  
 1204 data, including tilt and seismicity (Fig. 2).

1205 In models discussed above, the time-scale of pulsations  
 1206 depends principally on the volume of the magma cham-  
 1207 ber, magma rheology and the cross-sectional area of the  
 1208 conduit. These models might provide an explanation for  
 1209 the 2–3 year cycles of dome extrusion observed at SHV,  
 1210 where deformation data indicate that the magma chamber  
 1211 regulates the cycles. However, the models cannot simulta-  
 1212 neously explain the 5–7 week cycles. Thus another mech-  
 1213 anism is needed.

1214 The evidence for a dyke feeder at SHV includes  
 1215 GPS data [58], distribution of active vents, and seismic

1216 data [76]. We have assumed that, at depth, the conduit has  
 1217 an elliptical shape that transforms to a cylinder at shallow  
 1218 level. In order to get a smooth transition from the dyke at  
 1219 depth to a cylindrical conduit (see Fig. 1) the value of  $a_0$  in  
 1220 Eqs. (14) is parametrized as:

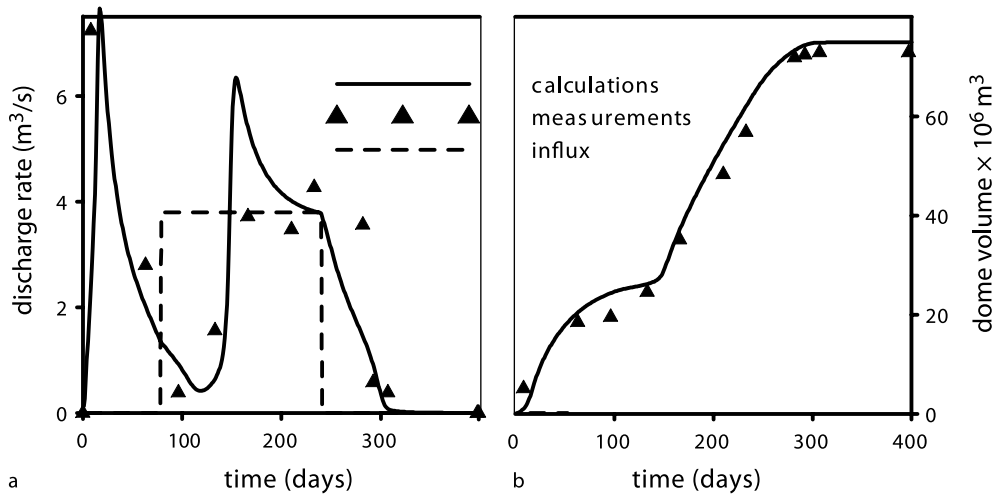
$$a_0(x) = A_1 \arctan\left(\frac{x - L_T}{w_T}\right) + A_2 \quad (21) \quad 1221$$

1222 Here  $L_T$  and  $w_T$  are the position and the vertical extent  
 1223 of the transition zone between the ellipse and the cylinder  
 1224 and constants  $A_1$  and  $A_2$  are calculated to satisfy condi-  
 1225 tions  $a_0(L) = R$  and  $a_0(0) = a_0$ , where  $R$  is the radius of  
 1226 the cylindrical part of the conduit and  $a_0$  is the length of  
 1227 semi-major axis at the inlet of the dyke. The value of  $b_0$   
 1228 is calculated in order to conserve the cross-section area of  
 1229 the unpressurized dyke, although it can also be specified  
 1230 independently.

1231 In order to de-couple the influence of the dyke geome-  
 1232 try from the oscillations caused by magma chamber pres-  
 1233 sure variations, we have assumed a fixed chamber pres-  
 1234 sure as a boundary condition for the entrance to the conduit.  
 1235 This assumption is valid because the timescale of chamber  
 1236 pressure variations are much longer than the period of the  
 1237 cycle (2–3 years in comparison with 5–7 weeks).

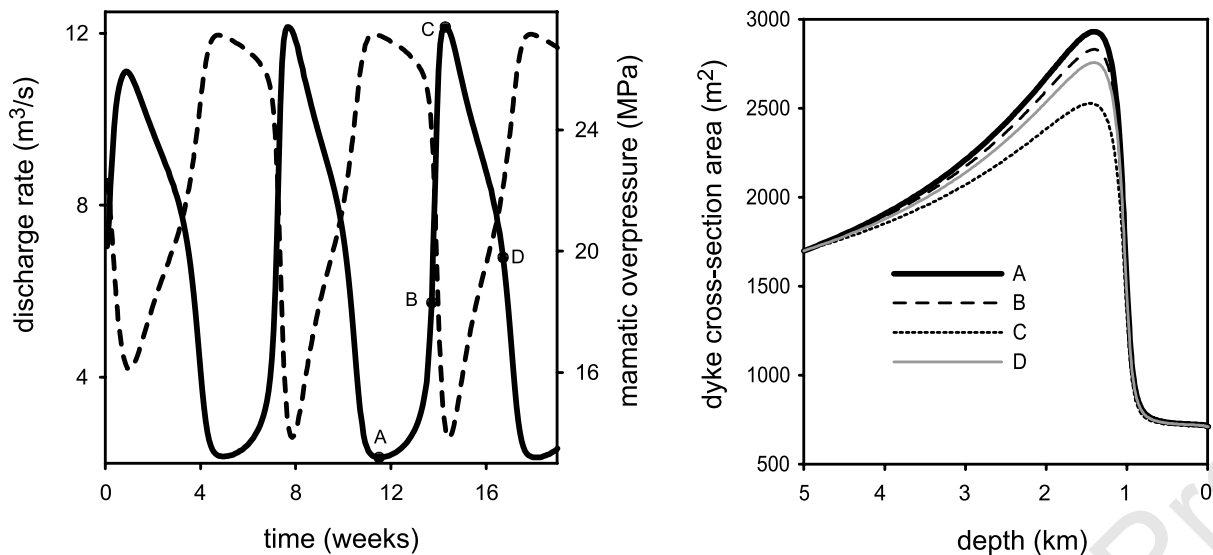
1238 Results presented in Figure 8 show that, even with  
 1239 a fixed chamber pressure, there are magma discharge rate  
 1240 oscillations. At the beginning of a cycle the magma dis-  
 1241 charge rate is at a minimum, while the overpressure (here





Volcanic Eruptions: Cyclicity during Lava Dome Growth, Figure 7

a Comparison of calculated and measured discharge rates (a) and volumes of the dome (b) for the episode of the dome growth in 2001–2002. Influx into the magma chamber is shown by a dashed line in a. Time in days begins on 6th June, 2001. After [25]



Volcanic Eruptions: Cyclicity during Lava Dome Growth, Figure 8

a Dependence of magma discharge rate (solid line) and magmatic overpressure at depth of 1 km (dashed line) on time, for  $a = 240$  m and  $b = 2.25$  m at the inlet of the dyke. The period of cycle is 46 days, average discharge rate is  $6.2 \text{ m}^3/\text{s}$ , with peak rate about  $12 \text{ m}^3/\text{s}$ . b Profiles of cross-section areas of the conduit during one cycle. Curve A corresponds to the beginning of the cycle, B – to a point on the curve of ascending discharge rate, C – to maximum discharge, and D to the middle of descending discharge curve. At the beginning of the cycle, due to large viscosity of magma (at low discharge rate crystal content is high) large magmatic overpressure develops, reaching a maximum near the transition between the dyke and cylindrical conduit; the dyke inflates providing temporary magma storage. Minimum dyke volume corresponds to maximum discharge rate (curve C). After [21]

1242 presented for 1 km depth by a dashed line) and dyke width  
 1243 are at a maximum. At point A in Fig. 8a the crystal content  
 1244 and viscosity have reached their maximum values. Beyond  
 1245 this threshold condition, an increase in magma discharge  
 1246 rate results in decreasing pressure and dyke width. How-

ever, crystal content and viscosity also decrease and this  
 effect decreases friction, resulting in flow rate increase and  
 pressure decrease. At C the system reaches minimum vis-  
 cosity and crystal content, which cannot decline further.  
 Thereafter the magma discharge rate decreases, while the

1247  
 1248  
 1249  
 1250  
 1251

1252 pressure and dyke width increase. The dyke acts like a capacitor, storing volume during this part of the cycle.  
1253

1254 The period of oscillation depends on several parameters such as influx rate and dyke aspect ratio  $a/R$ . Typically the period decreases with increasing aspect ratio. The range of calculated periods varies between 38 and 51 days for semi major-axis lengths,  $a$ , from 175 to 250 m and semi minor-axes,  $b$ , from 2 to 4 m. These results match observed cyclicity at SHV. The start of a cycle is quite sharp (Fig. 2), with the onset of shallow hybrid-type (impulsive, low-frequency coda) earthquakes. The change to shorter period and higher amplitude tilt pulsations indicate a marked increase in average magma discharge rate [91,98]. The model cycles also have rapid onsets. The high-amplitude tilt pulsations lasted for several weeks [91], consistent with the duration of higher magma discharge rates early in each 5–7 week cycle. Tilt data (Fig. 2) are consistent with the model in that the episode of high magma discharge is associated with a marked deflation that lasts several weeks (see dashed curve at Fig. 8, representing magmatic overpressure at 1 km depth). The magma pressure builds up in the swelling dyke and then reaches a threshold, whereupon a surge of partly crystallized magma occurs, accompanied by elevated seismicity.  
1275

1276 The models presented above have certain general features that are necessary to show cyclic behaviour. First of all, the resistance of the conduit must depend on magma discharge rate in a way that resistance decreases when discharge rate increases in some range of discharge rate. This dependence is reproduced by a sigmoidal curve. Resistance is a product of viscosity and velocity, and is linearly proportional to discharge rate. This means that magma viscosity must decrease as discharge rate strongly increases. There may be many reasons for this behaviour, including crystallization, temperature variation or gas diffusion. The second condition is that there must be some capacitor in the system that can store magma in a period of low discharge rate and release it in a period of high discharge rate. The role of this capacitor can be played by a magma chamber or dyke-shaped conduit located in elastic rocks, or by compressibility of the magma itself. The volumes of these capacitors are different and thus will cause pulsations with different periods. Currently there is no single model that can account for pulsations with multiple timescales.  
1296

### 1297 Future Directions

1298 Our models indicate that magmatic systems in lava dome eruptions can be very sensitive to small changes in parameters. This sensitivity is most marked when the system is

close to the cusps of steady-state solutions. If magma discharge rate becomes so high that gas cannot escape efficiently during magma ascent, then conditions for magma fragmentation and explosive eruption can arise. Empirical evidence suggests that conditions for explosive eruption arise when magma discharge rates reach approximately  $10 \text{ m}^3/\text{s}$  or more in dome eruptions [45,83]. Calculations show the possibility of such high discharge rates for the system parameters typical of lava dome-building eruptions.  
1310

We have illustrated model sensitivity of results by varying only one parameter at a time on plots of chamber pressure and discharge rate. However, magmatic systems have many controlling parameters that may vary simultaneously. Furthermore, some controlling parameters are likely to be interdependent (such as temperature, volatile content and phenocryst content, for example) and others may be independent (such as magma temperature and conduit dimensions). An eruption can be expected to move through  $n$ -parameter space, making simulation and its parameter depiction difficult. Our results are simplified, so system sensitivity and behaviour in the real world may be yet more complex. A volcanic system may be quite predictable when it is within a stable regime, but may become inherently unpredictable [84,85] when variations in the parameters move the system towards transition points and flow regime boundaries.  
1327

As in all complex systems there are many controlling parameters. Our models capture some of the key dynamics, but are still simplified in many respects, so do not fully capture the real variations. Our models do not, for example, consider variations in dome height, gas escape to surrounding rocks, strain-rate dependent rheological effects or time dependent changes in conduit diameter. The model for porosity is based on interpretation of measurements of porosity of erupted magma. The role of post-eruptive alterations of pore structure, for example, formation of cooling cracks, cannot be easily estimated. The model of bubble coalescence and permeability formation is important for understanding gas escape mechanisms and will provide constraints on transitions between extrusive and explosive activity. Because the model remains 1D, lateral distribution of parameters cannot be studied. These includes: lateral pressure gradients, magma crystallization on the conduit walls, wallrocks melting or erosion, formation of shear zones and shear heating, heat flux to surrounding rocks. The models also make the simplifying assumption that influx into the chamber from a deep source is a constant, or given as a function of time. The dynamics of the magma chamber itself are oversimplified in all existing conduit flow models. Changes in magma properties  
1351

in magma chamber can affect the long-term evolution of eruptions. We have considered water as the only volatile and the addition of other gas species (e. g. CO<sub>2</sub> and SO<sub>2</sub>) would add further variability.

There are large uncertainties in some parameters, which are likely to be very strong controls, such as the rheological properties of high crystalline magmas and crystal growth kinetic parameters, notably at low pressures (< 30 MPa) where experiments are very difficult to do (e. g. [22]). More experiments are necessary to understand the rheology of multiphase systems containing melt, crystals and bubbles. The effects of crystal shape, crystal size distribution and strain rate remain largely unclear. Some parameters, such as conduit geometry variation with depth, are highly uncertain. With so many parameters, good fits can be achieved by selecting plausible values for real systems. Barmin et al. [3], for example, were able to reproduce the patterns of discharge rate at Mount St. Helens and Santiaguito quite accurately. However, such models are not unique, partly because the actual values of some parameters may be quite different to the assumed values and partly because of the model simplifications.

Results obtained from waveform inversions of very-long-period seismic data over the past few years point to the predominance of a crack-like geometry for volcanic conduits [11], and it is becoming increasingly evident that the details of this geometry, such as conduit inclination, a sudden change in conduit direction, a conduit bifurcation, or a sudden increase in cross section, are all critically important in controlling magma flow dynamics. Future modeling attempts will need to be closely tied to information on conduit geometry derived from seismology to provide a more realistic view of volcanic processes.

The full simulation of any particular volcanic eruption in such a non-linear and sensitive system may appear a hopeless task. However, some reduction in uncertainties will certainly help to make the models more realistic. Further experimental studies of crystallization kinetics and the rheological properties of magma at high crystallinities are among the most obvious topics for future research. Advances in understanding the controls on magma input into an open-system chamber would be beneficial, since the delicate balance between input and output is a prime control on periodic behaviour.

Further model development includes 2D effects, elastic deformation effects in dyke-fed domes and coupling between magma chamber and conduit flow dynamics. Even with such improvements, large parameter uncertainties and modeling difficulties will remain. In such circumstances the logical approach is to start quantifying the uncertainties and sampling from them to produce probabilis-

tic outputs based on ensemble models where numerical models of the kind discussed here can be run many times. A future challenge for numerical models will also be to produce simulated outputs which compare in detail with observations, in particular time series of magma discharge rates.

### Acknowledgments

This work was supported by NERC research grant reference NE/C509958/1. OM and AB acknowledges Russian Foundation for Basic Research (05-01-00228) and President of Russian Federation program (NCH-4710.2006.1). RSJS acknowledges a Royal Society Wolfson Merit Award. The Royal Society exchange grants and NERC grants had supported the Bristol/Moscow work over the last 10 years.

### Bibliography

#### Primary Literature

- Balmforth NJ, Burbidge AS, Craster RV (2001) Shallow Lava Theory. In: Balmforth NJ, Provenzale A (eds) Geomorphological Fluid Mechanics. Lecture Notes in Physics, vol 582. Springer, Berlin, pp 164–187
- Balmforth NJ, Burbidge AS, Craster RV, Rust AC, Sassi R (2006) Viscoplastic flow over an inclined surface. *J Non-Newtonian Fluid Mech* 139:103–127
- Barmin A, Melnik O, Sparks RSJ (2002) Periodic behaviour in lava dome eruptions. *Earth Planet Sc Lett* 199:173–184
- Bingham EC (1922) Fluidity and Plasticity. McGraw-Hill, New York, p 215
- Blake S (1990) Viscoplastic models of lava domes. In: Fink JH (ed) Lava flows and domes, Vol 2. In: Fink JH (ed) Lava flows and domes; emplacement mechanisms and hazard implications. Springer, Berlin, pp 88–126
- Blundy JD, Cashman KV, Humphreys MCS (2006) Magma heating by decompression-driven crystallisation beneath andesite volcanoes. *Nature* 443:76–80. doi:10.1038/nature05100
- Calder ES, Lockett R, Sparks RSJ, Voight B (2002) Mechanisms of lava dome instability and generation of rockfalls and pyroclastic flows at Soufrière Hills Volcano, Montserrat. In: Druitt TH, Kokelaar BP (eds) The Eruption of Soufrière Hills Volcano, Montserrat, from 1995 to 1999, Geological Society, London, Memoirs No 21, pp 173–190
- Calder ES, Cortés JA, Palma JL, Lockett R (2005) Probabilistic analysis of rockfall frequencies during an andesite lava dome eruption: The Soufrière Hills Volcano, Montserrat. *Geophys Res Lett* 32:L16309. doi:10.1029/2005GL023594
- Caricchi L, Burlini L, Ulmer P, Gerya T, Vassalli M, Papale P (2007) Non-Newtonian rheology of crystal-bearing magmas and implications for magma ascent dynamics. *Earth Planet Sc Lett*, in press **CE2**
- Cashman KV, Blundy JD (2000) Degassing and crystallization of ascending andesite and dacite. In: Francis P, Neuberg J, Sparks RSJ (eds) Causes and consequences of eruptions of andesite volcanoes. *Phil Trans Royal Soc London A*, pp 1487–1513
- Chouet B, Dawson P, Arciniaga-Ceballos A (2005) Source mechanism of Vulcanian degassing at Popocatepetl Vol-

**CE2** Please update, if possible.

- cano, Mexico, determined from waveform inversions of very long period signals. *J Geophys Res* 110:B07301. doi:10.1029/2004JB003524
12. Christiansen RL, Peterson DW (1981) Chronology of the 1980 Eruptive Activity. In: Lipman PW, Mullineaux DR (eds) *The 1980 Eruptions of Mount St. Helens*. Washington, US Geological Survey Professional Paper 1250, p 844
13. Clarke AB, Stephens S, Teasdale R, Sparks RSJ, Diller K (2007) Petrological constraints on the decompression history of magma prior to Vulcanian explosions at the Soufrière Hills volcano, Montserrat. *J Volcanol Geotherm Res* 161:261–274. doi: 10.1016/j.jvolgeores.2006.11.007
14. Cole P, Calder ES, Sparks RSJ, Clarke AB, Druitt TH, Young SR, Herd R, Harford CL, Norton GE (2002) Deposits from dome-collapse and fountain-collapse pyroclastic flows at Soufrière Hills Volcano, Montserrat. In: Druitt TH, Kokelaar BP (eds) *The eruption of the Soufrière Hills Volcano, Montserrat from 1995 to 1999*. Geological Society, London, Memoir No 21, pp 231–262
15. Connor CB, Sparks RSJ, Mason RM, Bonadonna C, Young SR (2003) Exploring links between physical and probabilistic models of volcanic eruptions: the Soufrière Hills Volcano, Montserrat. *Geophys Res Lett* 30. doi:10.1029/2003GL017384
16. Costa A (2005) Viscosity of high crystal content melts: dependence on solid fraction. *Geophys Res Lett* 32:L22308. doi:10.1029/2005GL02430
17. Costa A, Macedonio G (2002) Nonlinear phenomena in fluids with temperature-dependent viscosity: an hysteresis model for magma flow in conduits. *Geophys Res Lett* 29(10). doi: 1029/2001GL014493
18. Costa A, Macedonio G (2003) Viscous heating in fluids with temperature-dependent viscosity: implications for magma flows. *Nonlinear Proc Geophys* 10:545–555
19. Costa A, Macedonio G (2005) Viscous heating in fluids with temperature-dependent viscosity: triggering of secondary flows. *J Fluid Mech* 540:21–38
20. Costa A, Melnik O, Sparks RSJ (2007) Controls of conduit geometry and wallrock elasticity on lava dome eruptions. *Earth Planet Sci Lett* 260:137–151. doi:10.1016/j.epsl.2007.05.024
21. Costa A, Melnik O, Sparks RSJ, Voight B (2007) The control of magma flow in dykes on cyclic lava dome extrusion. *Geophys Res Lett* 34:L02303. doi:1029/2006GL027466
22. Couch S, Sparks RSJ, Carroll MR (2001) Mineral disequilibrium in lavas explained by convective self-mixing in open magma chambers. *Nature* 411:1037–1039
23. Denlinger RP, Hoblitt RP (1999) Cyclic eruptive behaviour of silicic volcanoes. *Geology* 27(5):459–462
24. Diller K, Clarke AB, Voight B, Neri A (2006) Mechanisms of conduit plug formation: Implications for vulcanian explosions. *Geophys Res Lett* 33:L20302. doi:10.1029/2006GL027391
25. Dirksen O, Humphreys MCS, Pletchov P, Melnik O, Demyanchuk Y, Sparks RSJ, Mahony S (2006) The 2001–2004 dome-forming eruption of Shiveluch Volcano, Kamchatka: Observation, petrological investigation and numerical modelling. *J Volcanol Geotherm Res* 155:201–226. doi:10.1016/j.jvolgeores.2006.03.029
26. Druitt TH, Young S, Baptie B, Calder E, Clarke AB, Cole P, Harford C, Herd R, Luckett R, Ryan G, Sparks RSJ, Voight B (2002) Episodes of cyclic Vulcanian explosive activity with fountain collapse at Soufrière Hills volcano, Montserrat. In: Druitt TH, Kokelaar BP (eds) *The eruption of the Soufrière Hills Volcano, Montserrat from 1995 to 1999*. Geological Society, London, Memoir No 21, pp 231–262
27. Eichelberger JC, Carrigan CR, Westrich HR, Price RH (1986) Non-explosive silicic volcanism. *Nature* 323:598–602
28. Fedotov SA, Dvigalo VN, Zharinov NA, Ivanov VV, Seliverstov NI, Khubunaya SA, Demyanchuk YV, Markov LG, Osipenko LG, Smelov NP (2001) The eruption of Shiveluch volcano on May–July 2001. *Volcanol Seis* 6:3–15
29. Fink JH, Griffiths RW (1990) Radial spreading of viscous gravity currents with solidifying crust. *J Fluid Mech* 221:485–509
30. Fink JH, Griffiths RW (1998) Morphology, eruption rates, and rheology of lava domes: Insights from laboratory models. *J Geophys Res* 103:527–545
31. Green, DN, Neuberg J (2006) Waveform classification of volcanic low-frequency earthquake swarms and its implication at Soufrière Hills Volcano, Montserrat. *J Volcanol Geotherm Res* 153:51–63. doi:10.1016/j.jvolgeores.2005.08.003
32. Hale AJ, Bourgouin L, Mühlhaus HB (2007) Using the level set method to model endogenous lava dome growth. *J Geophys Res* 112:B03213. doi:10.1029/2006JB004445
33. Hale AJ, Wadge G (2003) Numerical modeling of the growth dynamics of a simple silicic lava dome. *Geophys Res Lett* 30(19). doi:10.1029/2003GL018182
34. Hammer JE, Rutherford MJ (2002) An experimental study of the kinetics of decompression-induced crystallization in silicic melt. *J Geophys Res* 107:(B1). doi:10.1029/2001JB000281
35. Harris AL, Rose WI, Flynn LP (2002) Temporal trends in Lava Dome extrusion at Santiaguito 1922–2000. *Bull Volcanol* 65:77–89
36. Hess KU, Dingwell DB (1996) Viscosities of hydrous leucogranite melts: A non-Arrhenian model. *Am Mineral* 81:1297–1300
37. Hoblitt RP, Wolfe EW, Scott WE, Couchman MR, Pallister JS, Javier D (1996) The preclimactic eruptions of Mount Pinatubo, June 1991. In: Newhall CG, Punongbayan RS (eds) *Fire and Mud: Eruptions and Lahars of Mount Pinatubo, Philippines*. Philippine Institute of Volcanology and Seismology, Quezon City, and University of Washington Press, Seattle, pp 457–511
38. Hort M (1998) Abrupt change in magma liquidus temperature because of volatile loss or magma mixing: effects of Nucleation, crystal growth and thermal history of the magma. *J Petrol* 39:1063–1076
39. Humphreys M, Blundy, JD, Sparks RSJ (2006) Magma Evolution and Open-system processes at Shiveluch Volcano: insights from phenocryst zoning. *J Petrol* 47:(12) 2303–2334. doi:10.1093/petrology/eg1045
40. Huppert HE, Shepherd JB, Sigurdsson H, Sparks RSJ (1982) On lava dome growth, with application to the 1979 lava extrusion of the Soufrière, St Vincent. *J Volcanol Geotherm Res* 14:199–222
41. Huppert HE, Woods AW (2002) The role of volatiles in magma chamber dynamics. *Nature* 420:493–495
42. Ida Y (1996) Cyclic fluid effusion accompanied by pressure change: Implication for volcanic eruptions and tremor. *Geophys Res Lett* 23:1457–1460
43. Iverson RM et al (2006) Dynamics of seismogenic volcanic extrusion at Mount St. Helens in 2004–05. *Nature* 444:439–443
44. Jaquet O, Sparks RSJ, Carniel R (2006) Magma Memory recorded by statistics of volcanic explosions at the Soufrière Hills Volcano, Montserrat. In: Mader HM, Coles SG, Connor CB,

**CE3** Is this the correct surname? Please check.



- 1575 Connor LJ (eds) *Statistics in Volcanology*. Geological Society, London, Special Publication of IAVCEI, vol 1. pp 175–184
- 1576
- 1577 45. Jaupart C, Allegre CJ (1991) Gas content, eruption rate and instabilities of eruption regime in silicic volcanoes. *Earth Planet Sci Lett* 102:413–429
- 1578
- 1579
- 1580 46. Kirkpatrick R (1976) Towards a Kinetic Model for the Crystallization of Magma Bodies. *J Geophys Res* 81:2565–2571
- 1581
- 1582 47. Landau L, Lifshitz E (1987) *Fluid Mechanics*, 2nd edn. Butterworth–Heinemann, Oxford
- 1583
- 1584 48. Lejeune A, Richet P (1995) Rheology of crystal-bearing silicate melts: An experimental study at high viscosity. *J Geophys Res* 100:4215–4229
- 1585
- 1586
- 1587 49. Lensky NG, Sparks RSJ, Navon O, Lyakhovsky V (2007) Cyclic activity at Soufriere Hills volcano, Montserrat. *J Volcanol Geotherm Res*, in review **CE2**
- 1588
- 1589
- 1590 50. Lister JR, Kerr RC (1991) Fluid mechanical models of crack propagation and their application to magma transport in dykes. *J Geophys Res* 96:10049–10077
- 1591
- 1592
- 1593 51. Llewellyn EW, Manga M (2005) Bubble suspension rheology and implications for conduit flow. *J Volcanol Geotherm Res* 143:205–217
- 1594
- 1595
- 1596 52. Loitsyansky LG (1978) *Fluid and gas mechanics*. Nauka, Moscow, pp 847 (in Russian)
- 1597
- 1598 53. Maeda I (2000) Nonlinear visco-elastic volcanic model and its application to the recent eruption of Mt. Unzen. *J Volcanol Geotherm Res* 95:35–47
- 1599
- 1600
- 1601 54. Mason RM, Starostin AB, Melnik O, Sparks RSJ (2006) From Vulcanian explosions to sustained explosive eruptions: The role of diffusive mass transfer in conduit flow dynamics. *J Volcanol Geotherm Res* 153:148–165. doi:10.1016/j.jvolgeores.2005.08.011
- 1602
- 1603
- 1604
- 1605
- 1606 55. Marsh BD (2000) Reservoirs of Magma and Magma chambers. In: Sigurdsson H (ed) *Encyclopedia of volcanoes*. Academic Press, New York, pp 191–206
- 1607
- 1608
- 1609 56. Mastin GL, Pollard DD (1988) Surface Deformation and Shallow Dike Intrusion Processes at Inyo Craters, Long Valley, California. *J Geophys Res* 93(B11):13221–13235
- 1610
- 1611
- 1612 57. Matthews SJ, Gardeweg MC, Sparks RSJ (1997) The 1984 to 1996 cyclic activity of Lascar Volcano, northern Chile: Cycles of dome growth, dome subsidence, degassing and explosive eruptions. *Bull Volcanol* 59:72–82
- 1613
- 1614
- 1615
- 1616 58. Mattioli G, Dixon TH, Farina F, Howell ES, Jansma PE, Smith AL (1998) GPS measurement of surface deformation around Soufriere Hills volcano, Montserrat from October 1995 to July 1996. *Geophys Res Lett* 25(18):3417–3420
- 1617
- 1618
- 1619
- 1620 59. Melnik O (2000) Dynamics of two-phase conduit flow of high-viscosity gas-saturated magma: large variations of sustained explosive eruption intensity. *Bull Volcanol* 62:153–170
- 1621
- 1622
- 1623 60. Melnik O, Barmin A, Sparks RSJ (2005) Dynamics of magma flow inside volcanic conduits with bubble overpressure buildup and gas loss through permeable magma. *J Volcanol Geotherm Res* 143:53–68
- 1624
- 1625
- 1626
- 1627 61. Melnik O, Sparks RSJ (1999) Non-linear dynamics of lava dome extrusion. *Nature* 402:37–41
- 1628
- 1629 62. Melnik O, Sparks RSJ (2002) Dynamics of magma ascent and lava extrusion at Soufrière Hills Volcano, Montserrat. In: Druitt TH, Kokelaar BP (eds) *The eruption of the Soufrière Hills Volcano, Montserrat from 1995 to 1999*. Geological Society, London, *Memoir No 21*, pp 223–240
- 1630
- 1631
- 1632
- 1633
63. Melnik O, Sparks RSJ (2005) Controls on conduit magma flow dynamics during lava dome building eruptions. *J Geophys Res* 110(B02209). doi:10.1029/2004JB003183
- 1634
- 1635
- 1636
64. Mériaux C, Jaupart C (1995) Simple fluid dynamic models of volcanic rift zones. *Earth Planet Sci Lett* 136:223–240
- 1637
- 1638
65. Murphy MD, Sparks SJ, Barclay J, Carroll MR, Brewer TS (2000) Remobilization origin for andesite magma by intrusion of mafic magma at the Soufrière Hills Volcano. In: *Montserrat WI (ed) A trigger for renewed eruption*. *J Petrol* 41:21–42
- 1639
- 1640
- 1641
- 1642
66. Muskhelishvili N (1963) *Some Basic Problems in the Mathematical Theory of Elasticity*. Noordhoff, Leiden, The Netherlands
- 1643
- 1644
67. Nakada S, Eichelberger JC (2004) Looking into a volcano: drilling Unzen. *Geotimes* 49:14–17
- 1645
- 1646
68. Nakada S, Shimizu H, Ohta K (1999) Overview of the 1990–1995 eruption at Unzen Volcano. *J Volcanol Geoth Res* 89:1–22
- 1647
- 1648
69. Navon O, Lyakhovsky V (1998) Vesiculation processes in silicic magmas. In: Gilbert J, Sparks RSJ (eds) *The Physics of explosive volcanic eruption*. Geological Society London, Special Publication, vol 145. pp 27–50
- 1649
- 1650
- 1651
- 1652
70. Neuberg JW, Tuffen H, Collier L, Green D, Powell T, Dingwell D (2006) The trigger mechanism of low-frequency earthquakes on Montserrat. *J Volcanol Geotherm Res* 153:37–50
- 1653
- 1654
- 1655
71. Newhall CG, Melson WG (1983) Explosive activity associated with the growth of volcanic domes. *J Volcanol Geoth Res* 17:111–131
- 1656
- 1657
- 1658
72. Norton GE, Watts RB, Voight B, Mattioli GS, Herd RA, Young SR, Devine JD, Aspinall WP, Bonadonna C, Baptie BJ, Edmonds M, Harford CL, Jolly AD, Loughlin SC, Luckett R, Sparks RSJ (2002) Pyroclastic flow and explosive activity of the lava dome of Soufrière Hills volcano, Montserrat, during a period of no magma extrusion (March 1998 to November 1999). In: Druitt TH, Kokelaar BP (eds) *The eruption of the Soufrière Hills Volcano, Montserrat from 1995 to 1999*. Geological Society, London, *Memoir No 21*, pp 467–482
- 1659
- 1660
- 1661
- 1662
- 1663
- 1664
- 1665
- 1666
- 1667
73. Ohba T, Kitade Y (2005) Subvolcanic hydrothermal systems: Implications from hydrothermal minerals in hydrovolcanic ash. *J Volcanol Geotherm Res* 145:249–262
- 1668
- 1669
- 1670
74. Robertson R, Cole P, Sparks RSJ, Harford C, Lejeune AM, McGuire WJ, Miller AD, Murphy MD, Norton G, Stevens NF, Young SR (1998) The explosive eruption of Soufriere Hills Volcano, Montserrat 17 September, 1996. *Geophys Res Lett* 25:3429–3432
- 1671
- 1672
- 1673
- 1674
- 1675
75. Roman DC (2005) Numerical models of volcanotectonic earthquake triggering on non-ideally oriented faults. *Geophys Res Lett* 32, doi:10.1029/2004GL021549
- 1676
- 1677
- 1678
76. Roman DC, Neuberg J, Luckett RR (2006) Assessing the likelihood of volcanic eruption through analysis of volcanotectonic earthquake fault-plane solutions. *Earth Planet Sci Lett* 248:244–252
- 1679
- 1680
- 1681
- 1682
77. Rubin AM (1995) Propagation of magma-filled cracks. *Annu Rev Planet Sci* 23:287–336
- 1683
- 1684
78. Saar MO, Manga M, Katharine VC, Fremouw S (2001) Numerical models of the onset of yield strength in crystal–melt suspensions. *Earth Planet Sci Lett* 187:367–379
- 1685
- 1686
- 1687
79. Sahagian D (2005) Volcanic eruption mechanisms: Insights from intercomparison of models of conduit processes. *J Volcanol Geotherm Res* 143(1–3): 1–15
- 1688
- 1689
- 1690
80. Slezin YB (1984) Dispersion regime dynamics in volcanic eruptions, 2. Flow rate instability conditions and nature of catastrophic explosive eruptions. *Vulkanol Seism* 1:23–35
- 1691
- 1692
- 1693

- 1694 81. Slezin YB (2003) The mechanism of volcanic eruptions  
1695 (a steady state approach). *J Volcanol Geotherm Res* 122:7–50  
1696 82. Sparks RSJ (1978) The dynamics of bubble formation and  
1697 growth in magmas – a review and analysis. *J Volcanol Geo-*  
1698 *therm Res* 3:1–37  
1699 83. Sparks RSJ (1997) Causes and consequences of pressurization  
1700 in lava dome eruptions. *Earth Planet Sci Lett* 150:177–189  
1701 84. Sparks RSJ (2003) Forecasting Volcanic Eruptions. *Earth and*  
1702 *Planetary Science Letters Frontiers in Earth Science Series*  
1703 *210:1–15*  
1704 85. Sparks RSJ, Aspinall WP (2004) Volcanic Activity: Frontiers and  
1705 Challenges. In: *Forecasting, Prediction, and Risk Assessment.*  
1706 *AGU Geophysical Monograph “State of the Planet” 150, IUGG*  
1707 *Monograph 19, pp 359–374*  
1708 86. Sparks RSJ, Murphy MD, Lejeune AM, Watts RB, Barclay J,  
1709 Young SR (2000) Control on the emplacement of the andesite  
1710 lava dome of the Soufrière Hills Volcano by degassing-induced  
1711 crystallization. *Terra Nova* 12:14–20  
1712 87. Sparks RSJ, Young SR (2002) The eruption of Soufrière Hills vol-  
1713 cano, Montserrat (1995–1999): overview of scientific results.  
1714 In: Druitt TH, Kokelaar BP (eds) *The eruption of the Soufrière*  
1715 *Hills Volcano, Montserrat from 1995 to 1999. Geological Soci-*  
1716 *ety, London, Memoir No 21, pp 45–69*  
1717 88. Sparks RSJ, Young SR, Barclay J, Calder ES, Cole PD, Darroux  
1718 B, Davies MA, Druitt TH, Harford CL, Herd R, James M, Leje-  
1719 une AM, Loughlin S, Norton G, Skeritt G, Stevens NF, Toothill  
1720 J, Wadge G, Watts R (1998) Magma production and growth of  
1721 the lava dome of the Soufrière Hills Volcano, Montserrat, West  
1722 Indies: November 1995 to December 1997. *Geophys Res Lett*  
1723 *25:3421–3424*  
1724 89. Swanson DA, Holcomb RT (1990) Regularities in growth of the  
1725 Mount St. Helens dacite dome 1980–1986. In: Fink JH (ed) *Lava*  
1726 *flows and domes; emplacement mechanisms and hazard im-*  
1727 *PLICATIONS. Springer, Berlin, pp 3–24*  
1728 90. Voight B, Hoblitt RP, Clarke AB, Lockhart AB, Miller AD, Lynch  
1729 L, McMahon J (1998) Remarkable cyclic ground deformation  
1730 monitored in real-time on Montserrat, and its use in eruption  
1731 forecasting. *Geophys Res Lett* 25:3405–3408  
1732 91. Voight B, Sparks RSJ, Miller AD, Stewart RC, Hoblitt RP, Clarke A,  
1733 Ewart J, Aspinall W, Baptie B, Druitt TH, Herd R, Jackson P, Lock-  
1734 hart AB, Loughlin SC, Lynch L, McMahon J, Norton GE, Robert-  
1735 son R, Watson IM, Young SR (1999) Magma flow instability and  
1736 cyclic activity at Soufrière Hills Volcano, Montserrat. *Science*  
1737 *283:1138–1142*  
1738 92. Walker GPL (1973) Lengths of lava flows. *Philos Trans Royal Soc*  
1739 *A 274:107–118*  
1740 93. Watson IM et al (2000) The relationship between degassing  
1741 and ground deformation at Soufrière Hills Volcano, Montser-  
1742 rat. *J Volcanol Geotherm Res* 98(1–4):117–126  
1743 94. Watts RB, Sparks RSJ, Herd RA, Young SR (2002) Growth pat-  
1744 terns and emplacement of the andesitic lava dome at Soufrière  
1745 Hills Volcano, Montserrat. In: Druitt TH, Kokelaar BP (eds) *The*  
1746 *eruption of the Soufrière Hills Volcano, Montserrat from 1995*  
1747 *to 1999. Geological Society, London, Memoir No 21, pp 115–*  
1748 *152*  
1749 95. Whitehead JA, Helfrich KR (1991) Instability of flow with tem-  
1750 perature-dependent viscosity: a model of magma dynamics.  
1751 *J Geophys Res* 96:4145–4155  
1752 96. Williams SN, Self S (1983) The October 1902 Plinian eruption  
1753 of Santa Maria volcano, Guatemala. *J Volcanol Geotherm Res*  
1754 *16:33–(Melnik and Sparks, 2005) CE4*
97. Woods AW, Koyaguchi T (1994) Transitions between explosive  
and effusive eruption of silicic magmas. *Nature* 370:641–645 1755  
1756  
98. Wylie JJ, Voight B, Whitehead JA (1999) Instability of magma  
flow from volatile-dependent viscosity. *Science* 285:1883–  
1757 1885 1758  
1759  
99. Yokoyama I, Yamashita H, Watanabe H, Okada H CE5 Geophys-  
ical characteristics of dacite volcanism – 1977–1978 eruption  
of Usu volcano. *J Volcanol Geotherm Res* 9:335–358 1760  
1761  
1762

**Books and Reviews**

- Dobran F (2001) *Volcanic Processes: Mechanisms In Material Trans-*  
port. Springer, CE6 pp 620 1763  
1764  
Gilbert JS, Sparks RSJ (eds) (1998) *The Physics of Explosive Volcan-*  
ism. Special Publication of the Geological Society of London,  
pp 186 CE7 1765  
1766  
Gonnermann H, Manga M (2007) The fluid mechanics inside a vol-  
cano. *Ann Rev Fluid Mech* 39:321–356 1767  
1768  
Mader HM, Coles SG, Connor CB, Connor LJ (2006) *Statistics in Vol-*  
canology. IAVCEI Publications, Geological Society Publishing  
House, p 296 1769  
1770  
1771  
1772  
1773

CE4 Please provide the correct page range.

CE5 Please provide the year.

CE6 Please provide the publisher location.

CE7 Please provide volume number.